Journal of Virology

| Editor's Pick | Host-Microbial Interactions | Full-Length Text

Zika virus infection leads to hormone deficiencies of the hypothalamic-pituitary-gonadal axis and diminished fertility in mice

Li-Bo Liu,[1] Wei Yang,[1,2] Jia-Tong Chang,[1] Dong-Ying Fan,[1] Yan-Hua Wu,[1] Pei-Gang Wang,[1] Jing An[1,3]

AUTHOR AFFILIATIONS See affiliation list on p. 22.

ABSTRACT Zika virus (ZIKV) infection in pregnant women during the first trimester can cause congenital malformations including microcephaly, which has focused global attention on this emerging pathogen. By contrast, ZIKV infection in pregnant women during the third trimester can cause neurodevelopmental delays and cryptorchidism in newborns without microcephaly. Here, we evaluated the long-term fertility consequences of ZIKV infection in male suckling mice, which is equivalent to congenital ZIKV infection in children, from multiple perspectives including the hypothalamic-pituitary-gonadal axis, testis, sperm, and social behaviors. We observed the persistence of ZIKV in the hypothalamus of mice, which caused long-term hormone deficiencies of the hypothalamic-pituitary-gonadal axis. Hormone deficiencies led to limited delays in testicular development, a decrease in sperm quality and quantity, and abnormal social abilities. These damages could progress to diminished fertility in male mice, as judged by lower pregnancy rate, prolonged time to delivery, and decreased offspring quality. Currently, the extent to which these observations in mice translate to humans remains unclear, but longitudinal studies of hormone levels and reproductive health in ZIKV-exposed children seem warranted.

IMPORTANCE Zika virus (ZIKV) infection in pregnant women during the third trimester can cause neurodevelopmental delays and cryptorchidism in children without microcephaly. However, the consequences of congenital ZIKV infection on fertility in these children remain unclear. Here, using an immunocompetent mouse model, we reveal that congenital ZIKV infection can cause hormonal disorders of the hypothalamic-pituitary-gonadal axis, leading to reduced fertility and decreased sexual preference. Our study has for the first time linked the hypothalamus to the reproductive system and social behaviors after ZIKV infection. Although the extent to which these observations in mice translate to humans remains unclear, these findings did suggest that the reproductive health and hormone levels of ZIKV-exposed children should receive more attention to improve their living quality.

KEYWORDS Zika virus, hypothalamus, hormone deficiencies, developmental delays, testis, fertility

Zika virus (ZIKV), a member of mosquito-borne flaviviruses, is primarily transmitted by Aedes mosquitoes (1); however, sexual transmission and vertical transmission of ZIKV have been reported (2). ZIKV was first discovered in the Zika jungle of Uganda, Africa in 1947 (3), and emerged as a public health concern during the ZIKV epidemic from the Asia-Pacific region to the Americas in 2015–2017 (4, 5). ZIKV affected millions of people in 87 countries and territories, caused thousands of microcephaly cases, and aggravated the disease burden on countless families (6, 7).

Editor Mark T. Heise, University of North Carolina at Chapel Hill, Chapel Hill, North Carolina, USA

Address correspondence to Pei-Gang Wang, pgwang@ccmu.edu.cn, or Jing An, anjing@ccmu.edu.cn.

The authors declare no conflict of interest.

See the funding table on p. 23.

Received 6 July 2023
Accepted 3 August 2023
Published 21 September 2023

ZIKV infection in pregnant women during the first trimester can cause congenital malformations including microcephaly (8–10). By contrast, ZIKV infection of pregnant women during the third trimester receives little attention because their newborns did not exhibit apparent congenital malformations (11). Epidemiological investigations indicated that these newborns also had a variety of developmental complications (12–17). In Brazil, an investigation of 115 three-month-old neonates showed that 56 ZIKV-exposed neonates had significantly lower weight and body length than 59 non-exposed neonates (15). Recent studies also revealed that the majority of ZIKV-exposed children had developmental delays in cognition, language, motor, and adaptation, especially social-emotional abilities from 7 to 32 months old (12–14). In 2019, an investigation of 22 male children exposed to ZIKV showed that 8 of them had cryptorchidism (17). These studies suggested that ZIKV infection can cause various developmental delays in newborns, but the long-term consequences of neonatal ZIKV infection on their reproductive health remain unclear.

In our previous study, using ZIKV-infected suckling mice, we observed that ZIKV infection in the hypothalamus caused hormone deficiencies along the hypothalamic-pituitary-thyroid axis, resulting in irreversible growth delay and memory impairment (18). As the superior center of the neuroendocrine system, the hypothalamus also plays an important role in fertility by regulating the hypothalamic-pituitary-gonadal (HPG) axis. Thus, whether ZIKV infection affects reproductive development via the HPG axis remains unclear. In the current study, using ZIKV-infected male suckling mice, we observed that ZIKV infection caused long-term hormone deficiencies of the HPG axis, accompanied by phenotypes associated with reproductive endocrine disorders in mice. The impacts of ZIKV infection on the reproductive endocrine system and fertility persisted up to the adulthood of mice. Thus, our results provided clues to appreciate the potential impacts of ZIKV infection on the reproductive health and hormone levels of children in the epidemic area.

RESULTS

Postnatal ZIKV infection causes diminished fertility in male mice

Male suckling mice were intracerebrally inoculated with ZIKV at postnatal day 2 (P2), which is equivalent to the neonatal infection during the third trimester (19, 20). Compared with control mice, ZIKV-infected male mice had significantly lower body weight from 7 to 56 days post-infection (dpi) (Fig. 1A), and 43.3% of them survived more than 6 weeks (Fig. 1B). In addition, ZIKV-infected mice had remarkably lower weights of brain, heart, lung, liver, kidney, and testes (Fig. 1C through F).

To determine whether postnatal ZIKV infection affects fertility in male mice, ZIKV-infected male mice were mated with healthy age-matched female mice when they were 6 or 8 weeks old (Fig. 2A through L). The pregnancy rate, the time from being co-caged to delivery, and the litter size were recorded. Although 68.75% (11/16, 6 weeks old) or 79% (19/24, 8 weeks old) of female mice in cages with ZIKV-infected male mice were able to become pregnant (Fig. 2A and G), they had significantly longer time (up to 53 days) to delivery (Fig. 2B and H). ZIKV-infected mice also had fewer litter sizes than control mice (Fig. 2C and I). In addition, we observed noticeably lower birth weight, lower 4-week weight, and more females in offspring of ZIKV-infected mice (Fig. 2D through F and J through L). These results indicated decreased fertility in postnatal ZIKV-infected mice in adulthood.

Limited developmental delays in testes of ZIKV-infected mice

The testis is a key organ for spermatogenesis. To determine whether the diminished fertility results from ZIKV-induced damage to testes, we evaluated pathological changes in mouse testes. We observed smaller testes in ZIKV-infected mice than in control mice at 14, 28, and 56 dpi (Fig. 3A and B), while the testis organ coefficient was similar in the two groups (Fig. 1E and F). ZIKV RNA was detected in part (2/5) of mouse testes only at 7 dpi

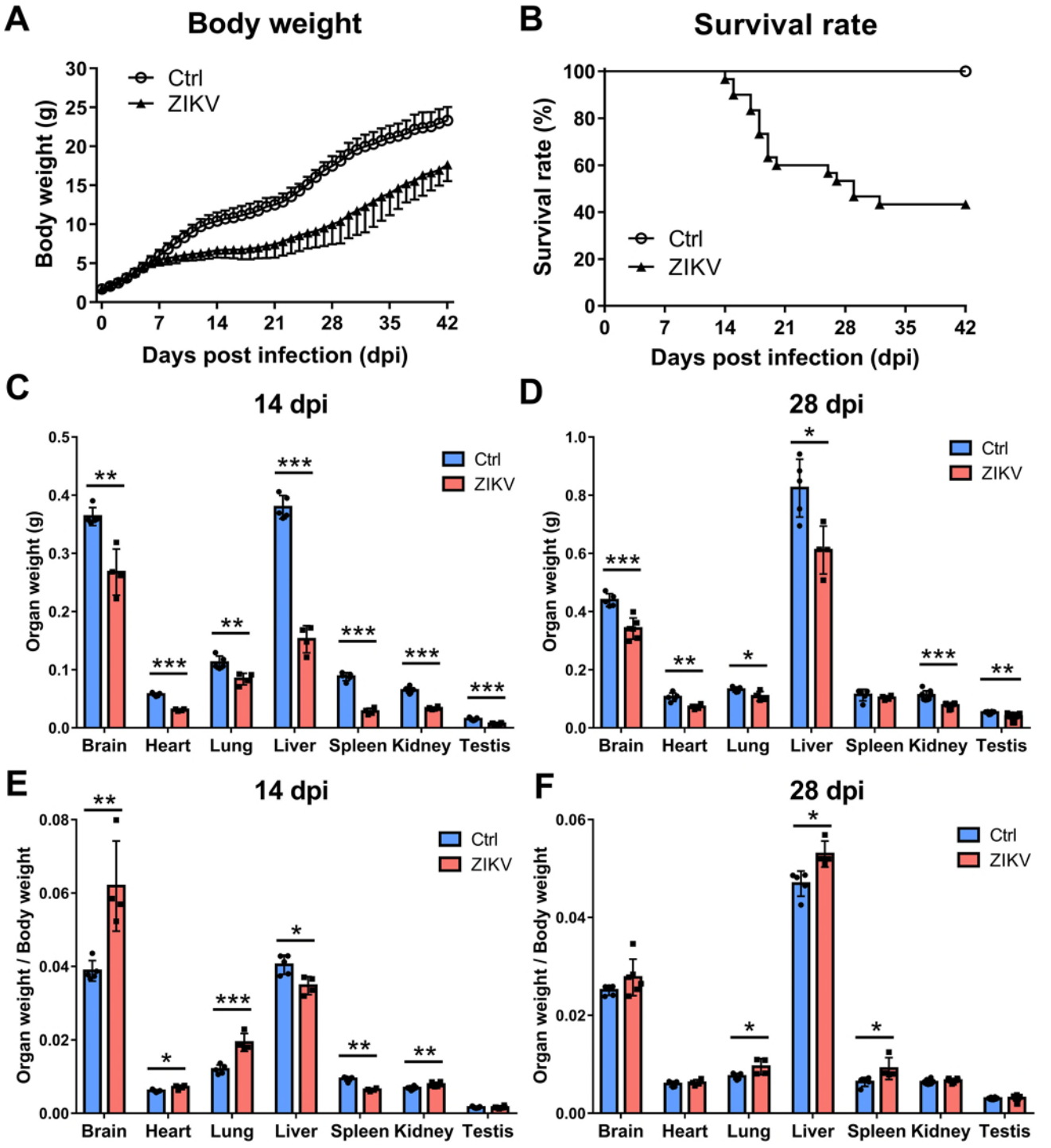

FIG 1 Body weight, survival rate, organ weight, and organ coefficient of neonatal ZIKV-infected mice. BALB/c male mice at postnatal day 2 were intracerebrally inoculated with 100 plaque-forming units of ZIKV or phosphate-buffered saline. (A) Body weight and (B) survival rate were inspected daily for 42 days after infection ($n = 11$ for the Ctrl group; $n = 30$ for the ZIKV group). (C and D) Weight of brain, heart, lung, liver, spleen, kidney, and testis in ZIKV-infected and control mice ($n = 4$ to 5 for each time point) at (C) 14 dpi and (D) 28 dpi. (E and F) Organ coefficients of brain, heart, lung, liver, spleen, kidney, and testis in ZIKV-infected and control mice at (E) 14 dpi and (F) 28 dpi. (*$P < 0.05$; **$P < 0.01$; ***$P < 0.001$; Student's *t*-test).

(Fig. 3C). These results indicated that the testicular development was coordinated with the overall development in ZIKV-infected mice. A few mice had transient testicular infections, which was similar to the detection rate of ZIKV in men's semen, as reported (21).

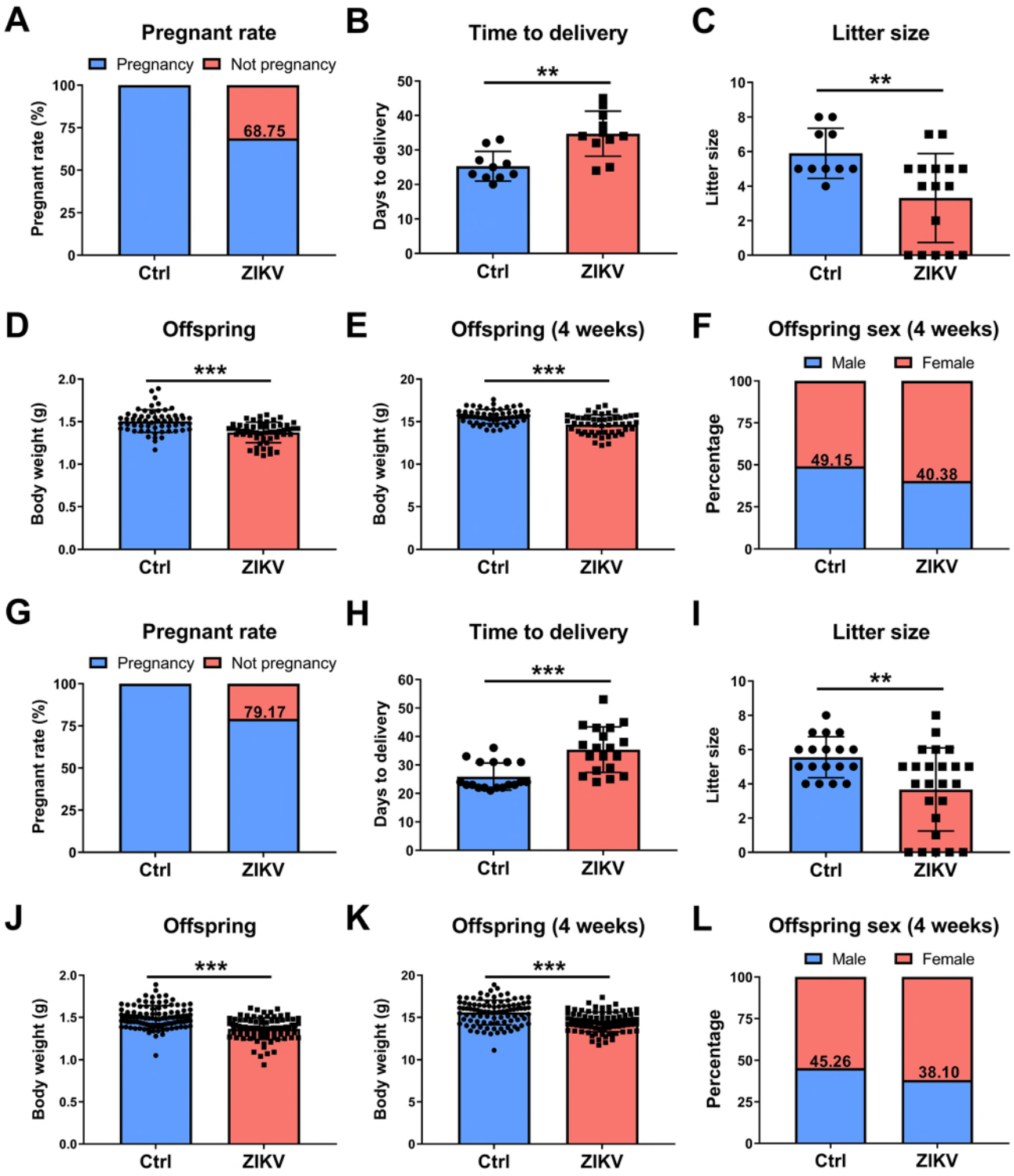

FIG 2 Mating experiments of neonatal ZIKV-infected mice at 6 and 8 weeks old. 6-week-old and 8-week-old ZIKV-infected and control male mice were mated with healthy age-matched female mice in a ratio of 1:2. (A) Pregnant rate, (B) the time from being co-caged to delivery of female mice, (C) the litter size, (D) birth weight, (E) body weight at 4 weeks, and (F) the sex ratio of offspring mice were recorded in mating experiments of 6-week-old mice (n = 5 for the Ctrl group; n = 8 for the ZIKV group). (G) Pregnant rate, (H) the time from being co-caged to delivery of female mice, (I) the litter size, (J) birth weight, (K) body weight at 4 weeks, and (L) the sex ratio of offspring mice were recorded in mating experiments of 8-week-old mice (n = 9 for the Ctrl group; n = 12 for the ZIKV group). (**P < 0.01; ***P < 0.001; Mann-Whitney U test for the litter size; Student's t-test for others).

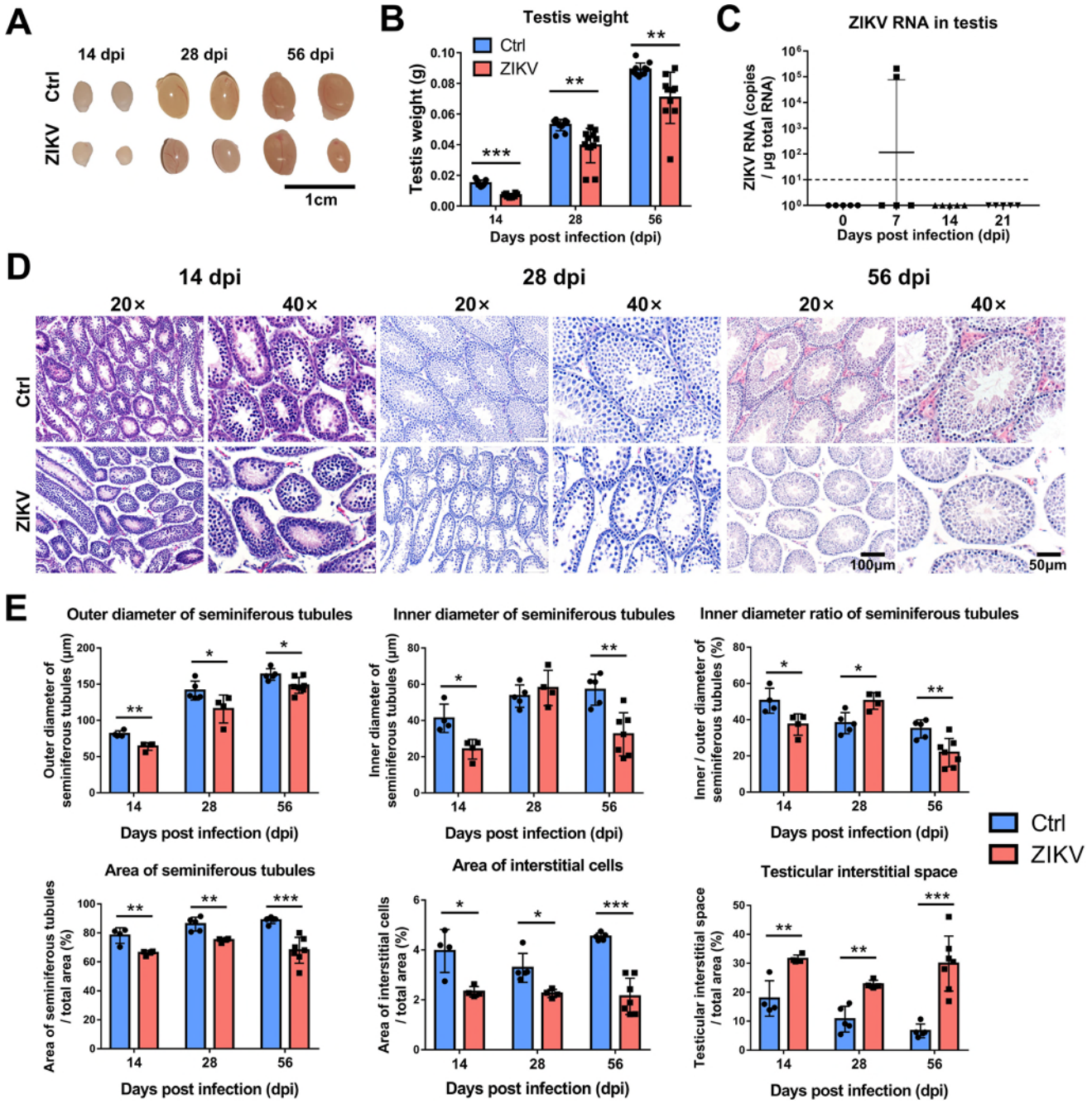

FIG 3 Effects of neonatal ZIKV infection on mice testes. Testes were collected from ZIKV-infected and control mice at 14, 28, and 56 dpi (n = 5 to 6 male mice for each time point). (A) Representative images of testis from ZIKV-infected and control mice at 14, 28, and 56 dpi; scale bar = 1 cm. (B) Testis weight from ZIKV-infected and control mice at 14, 28, and 56 dpi (**P < 0.01; ***P < 0.001; Student's t-test). (C) Testes collected were analyzed for viral RNA by RT-qPCR. The dashed line indicates the detection limit. (D) Hematoxylin and eosin (HE) staining of testes sections collected from ZIKV-infected and control mice at 20× (left) and 40× (right) magnification. (E) Outer diameter, inner diameter, diameter ratio, area of seminiferous tubules, area of interstitial cells, and interstitial space were measured from HE staining of testes sections (*P < 0.05; **P < 0.01; ***P < 0.001; Student's t-test).

Hematoxylin and eosin (HE) staining showed atrophy of seminiferous tubules in the testes of ZIKV-infected mice, as judged by irregular tubule morphology, reduced outer diameter, and extended interstitium between seminiferous tubules (Fig. 3D and E). Over time, seminiferous tubules of ZIKV-infected mouse testes became more regular morphology, and their spermatogenic cells increased (Fig. 3D and E). There was no obvious inflammatory cell infiltration and loss of integrity of the blood-testis-barrier (BTB) in the

testis of ZIKV-infected mice. These results indicated that testes of postnatal ZIKV-infected mice were not severely damaged, albeit developmental delays, which is distinct from severe destruction observed in ZIKV-infected Ifnar1$^{-/-}$ mice (22, 23) or C57BL/6 mice treated with anti-Ifnar1 blocking monoclonal antibody (24).

Immunofluorescence staining for DDX4 (a spermatogenic cell marker) and SOX9 (a Sertoli cell marker) was performed to examine the number and distribution of spermatogenic cells and Sertoli cells in the testes. At 14 dpi, ZIKV-infected and control mice had similar numbers of DDX4^{+} cells, while SOX9^{+} cells were not observed in ZIKV-infected mice (Fig. 4A and B). Subsequently, ZIKV-infected mice had significantly fewer DDX4^{+} and SOX9^{+} cells than control mice at 28 dpi; however, there was no statistical difference between the two groups at 56 dpi (Fig. 4A and B). These results indicated reversible developmental delays of spermatogenic cells and Sertoli cells in the testes of ZIKV-infected mice.

Papanicolaou staining for sperm smears harvested from epididymis at 56 dpi showed significantly less sperm in ZIKV-infected mice compared with control mice (Fig. 4C and D). ZIKV-infected mice had a higher rate of abnormal sperm (e.g., capitulum, headless, angular neck, double tail, and short tail) (Fig. 4D). These results indicated the decreased quantity and quality of sperm in ZIKV-infected mice.

Taken together, testes of postnatal ZIKV-infected mice had limited developmental delays, which was distinct from severe destruction observed in testes of ZIKV-infected C57BL/6 mice treated with anti-Ifnar1 blocking monoclonal antibody (24) or ZIKV-infected Ifnar1$^{-/-}$ mice (22, 23). Thus, the longer time to delivery, diminished fertility, and decreased offspring quality in ZIKV-infected mice were most likely due to the decrease in sperm quantity and quality, rather than the damage of ZIKV to the testes.

Reduced sociability and preference for females in ZIKV-infected mice

To determine whether ZIKV infection affects social behavior in mice, we used the three-chamber task to inspect the voluntary initiation of social interaction and preference for social novelty of mice (Fig. 5A). In the sociability phase, one partner (Stranger 1) was placed in a chamber on one side, and the chamber on the other side was empty. Control mice tended to spend more time in the chamber with social partner and barely entered the empty chamber. By contrast, ZIKV-infected mice spent significantly more time in the empty chamber (Fig. 5B). In the social novelty phase, a novel partner (Stranger 2) was introduced into the previously empty chamber. Control mice exhibited a preference for the novel partner (Stranger 2), while ZIKV-infected mice displayed a preference for the familiar partner (Stranger 1) (Fig. 5B). ZIKV-infected mice had a remarkably lower index of social novelty preference (Fig. 5B). These results suggested that ZIKV-infected mice had reduced sociability and preference for social novelty.

Next, we used the open field test to evaluate the motor ability and autonomous exploration ability of mice (Fig. 5C). Each test mouse was placed in a 50 × 50 cm square cage to move freely. Compared with control mice, ZIKV-infected mice had longer distance traveled, fewer freezing episodes, less freezing time, and higher maximum speed (Fig. 5D and E). ZIKV-infected mice spent more time traveling in the central area than control mice and spent less time traveling in the peripheral area (Fig. 5D and E). These results indicated reduced autonomous exploration behavior and increased aimless running in ZIKV-infected mice, while their motor ability was normal.

Finally, we used the three-chamber task to evaluate whether ZIKV infection altered the sexual preference of male mice leading to prolonged time to delivery. One male partner and one female partner were, respectively, introduced into the left and right chambers (Fig. 5F). Control male mice consistently entered the female chamber and kept sniffing with the female partner at all times (Fig. 5G). By contrast, ZIKV-infected male mice shuttled repeatedly through three chambers, and they spent significantly less time sniffing with the female partner (Fig. 5G). These results indicated that ZIKV-infected male mice exhibited a decreased preference for female mice, which might cause reduced mating behavior and thus prolonged time to delivery.

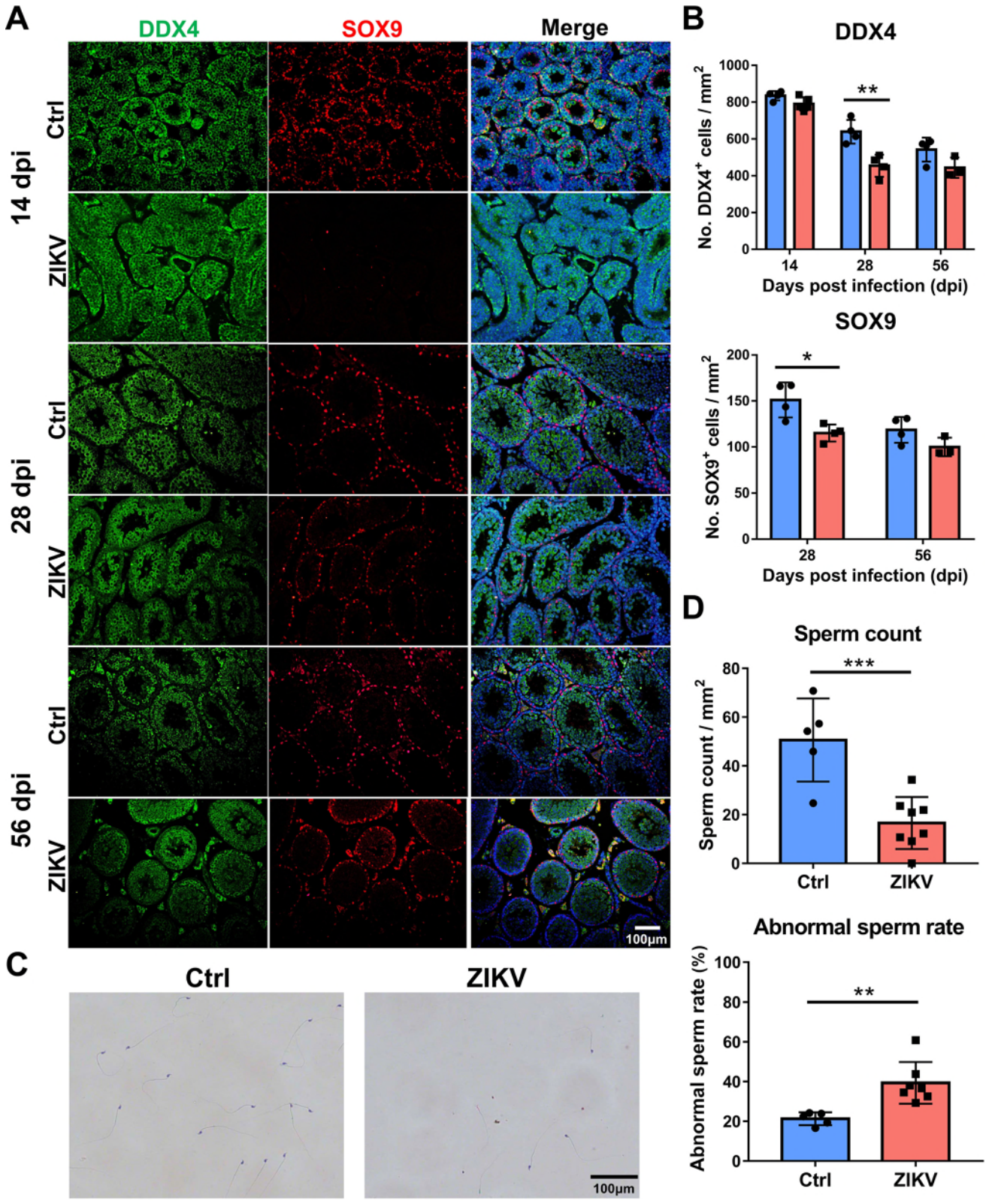

FIG 4 Effects of neonatal ZIKV infection on testes and sperm of mice. (A) Immunofluorescence (IF) staining of testes sections collected from ZIKV-infected and control mice with antibodies to DDX4 (spermatogenic cells) and SOX9 (Sertoli cells). Scale bars = 100 μm. (B) The number of DDX4$^+$ cells and SOX9$^+$ cells was counted from IF staining of testes sections (*P < 0.05; **P < 0.01; Student's t-test). (C) Papanicolaou staining of sperm smears harvested from the epididymis of ZIKV-infected and control mice at 56 dpi. Scale bars = 100 μm. (D) Sperm count and abnormal sperm rate were counted from Papanicolaou staining of sperm smears (**P < 0.01; ***P < 0.001; Student's t-test).

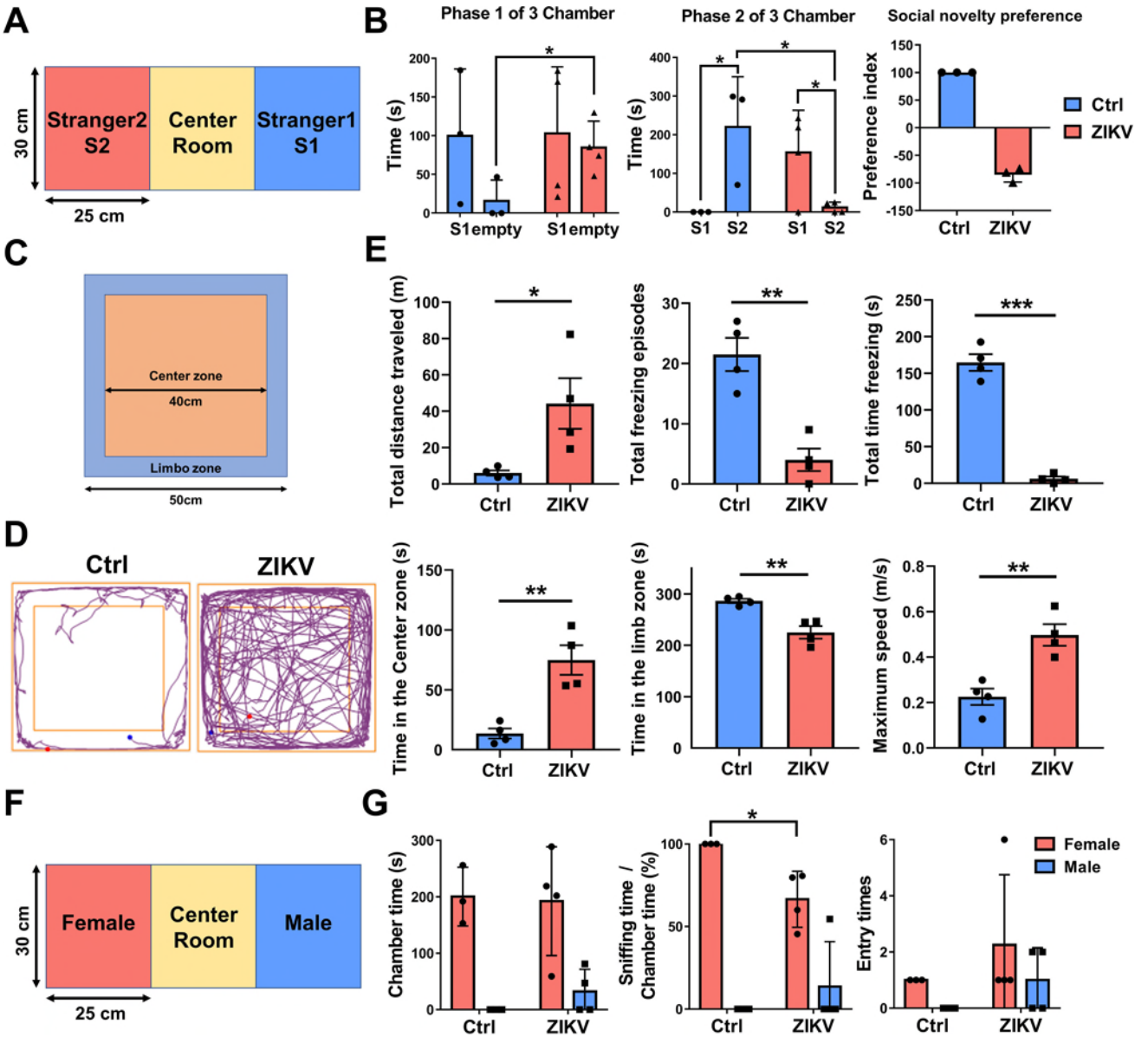

FIG 5 Neonatal ZIKV infection caused abnormal behaviors in mice. (A) Schematic diagram of the three-chamber task to evaluate social behavior and social novelty preference of mice. (B) The time spent on socializing with Stranger 1 or Stranger 2 and index of social novelty preference for ZIKV-infected and control mice (n = 3 to 4) at 12 weeks during the three-chamber task (*P < 0.05; Student's t-test). (C) Schematic diagram used in the open field test to evaluate the motor ability and autonomous exploration. (D) Representative moving tracks of ZIKV-infected and control mice at 12 weeks. (E) Statistics of total distance traveled, total freezing episodes, total time freezing, time in the center zone, time in the limb zone, and the maximum speed of ZIKV-infected and control mice (n = 4) during the open field test (*P < 0.05; **P < 0.01; ***P < 0.001; Student's t-test). (F) Schematic diagram of the three-chamber task to evaluate the sex preference of male mice. (G) Statistics of the chamber time, sniffing time, and entry times of ZIKV-infected and control mice (n = 3 to 4) at 12 weeks during the three-chamber task (*P < 0.05; Student's t-test).

ZIKV infection in the hypothalamus causes long-term hormone deficiencies in the HPG axis

The hypothalamus regulates hormone production via the HPG axis, affecting reproductive development and mating behavior. To determine whether ZIKV infection affects hormone secretion of the HPG axis, we used enzyme-linked immunosorbent assay (ELISA) to assay serum concentration of four hormones, including gonadotropin-releasing hormone (GnRH), follicle-stimulating hormone (FSH), luteinizing hormone (LH), and testosterone. Compared with control mice, ZIKV-infected mice had significantly lower

GnRH concentrations from 7 to 56 dpi (Fig. 6A), and lower FSH and LH concentrations from 14 to 56 dpi (Fig. 6B and C). Control mice had two peaks of testosterone concentrations at 7 and 56 dpi, which is consistent with physiological testosterone surges as reported (25). By contrast, ZIKV-infected mice displayed sustained high levels of testosterone concentration, which was slightly below the testosterone peaks of control mice (Fig. 6D). These results indicated long-term hormone deficiencies of the HPG axis in ZIKV-infected mice.

To determine the mechanisms underlying hormone deficiencies of the HPG axis, we examined the hypothalamus and pituitary in mice. ZIKV RNA was detected in the hypothalamus from 7 to 14 dpi (Fig. 7A), while it was undetectable in the pituitary at any time point. Colocalization of ZIKV and GnRH$^+$ cells was also observed in the hypothalamus of mice at 7 dpi (Fig. 7B). ZIKV-infected mice displayed reduced GnRH RNA in the hypothalamus than control mice from 14 to 56 dpi (Fig. 7C). Immunohistochemical staining also revealed a reduced area of GnRH$^+$ cell mass in the hypothalamus of ZIKV-infected mice (Fig. 7D). ZIKV-infected mice showed lighter staining for FSH and LH in the pituitary (Fig. 8). These results indicated that ZIKV could infect the hypothalamus of mice, causing delays in neuroendocrine development and decreased hormone expressions of the HPG axis.

Oxytocin secreted by the hypothalamus can regulate social behavior (26, 27). To determine whether ZIKV infection affects oxytocin production, we used immunostaining for oxytocin. The hypothalamus and pituitary of ZIKV-infected mice displayed

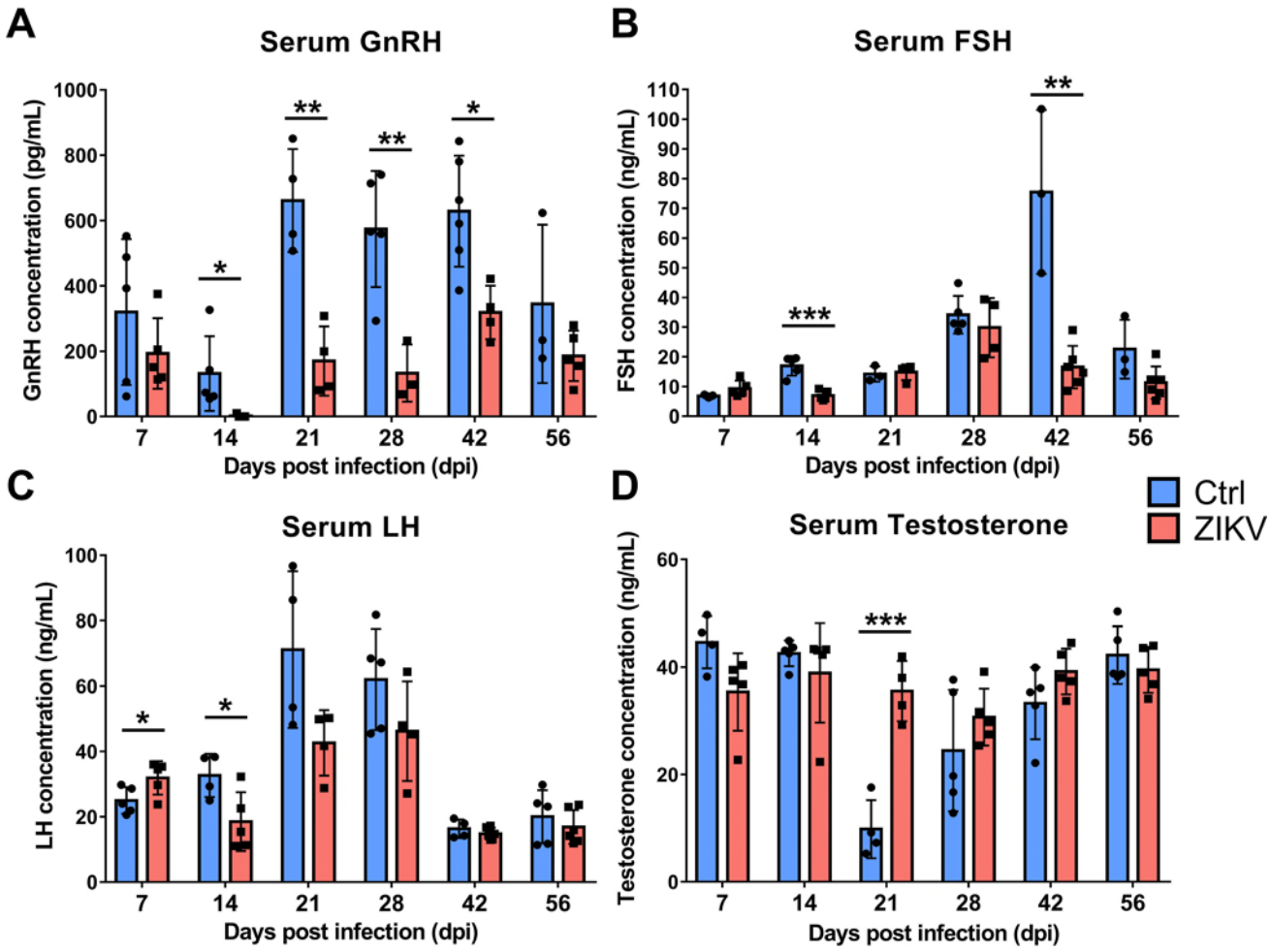

FIG 6 Serum GnRH, FSH, LH, and testosterone concentrations of ZIKV-infected and control mice (n = 3 to 6 for each time point) determined by ELISA (*P < 0.05; **P < 0.01; ***P < 0.001; Student's t-test).

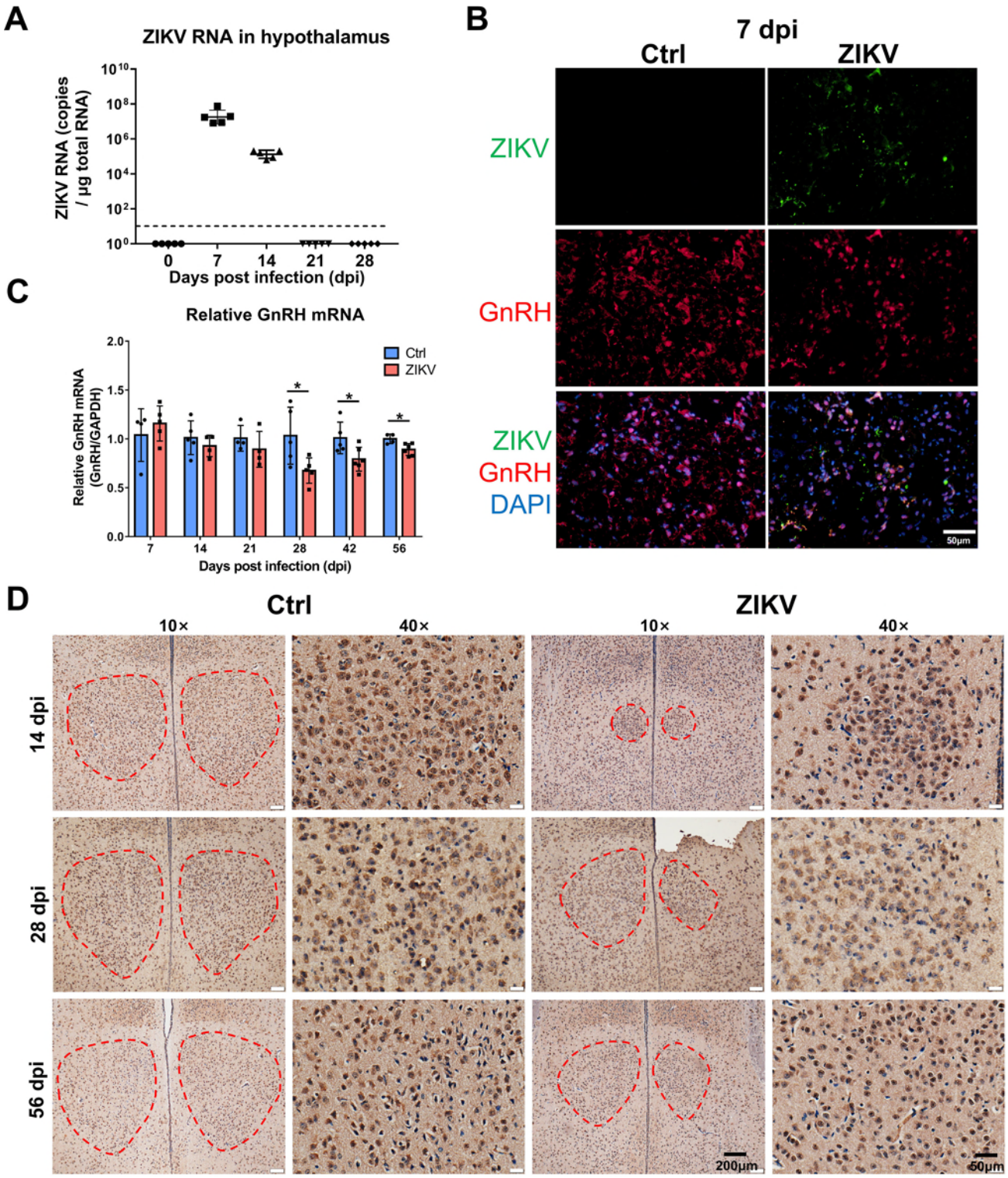

FIG 7 ZIKV infection in the hypothalamus caused decreased GnRH expression in mice. (A) Hypothalamus collected from ZIKV-infected mice (n = 5 for each time point) were analyzed for viral RNA by RT-qPCR. The dashed line indicates the detection limit. (B) Immunofluorescence staining for ZIKV and GnRH in the hypothalamus of ZIKV-infected and control mice at 7 dpi. (C) The relative GnRH mRNA expression in the hypothalamus of ZIKV-infected and control mice (n = 4 to 6 for each time point) was assayed by RT-qPCR (*P < 0.05; Student's t-test). (D) Immunohistochemical staining for GnRH in the hypothalamus of ZIKV-infected and control mice at 10× (left) and 40× (right) magnification. Red dashed circles indicate the area of $GnRH^+$ neuroendocrine cells.

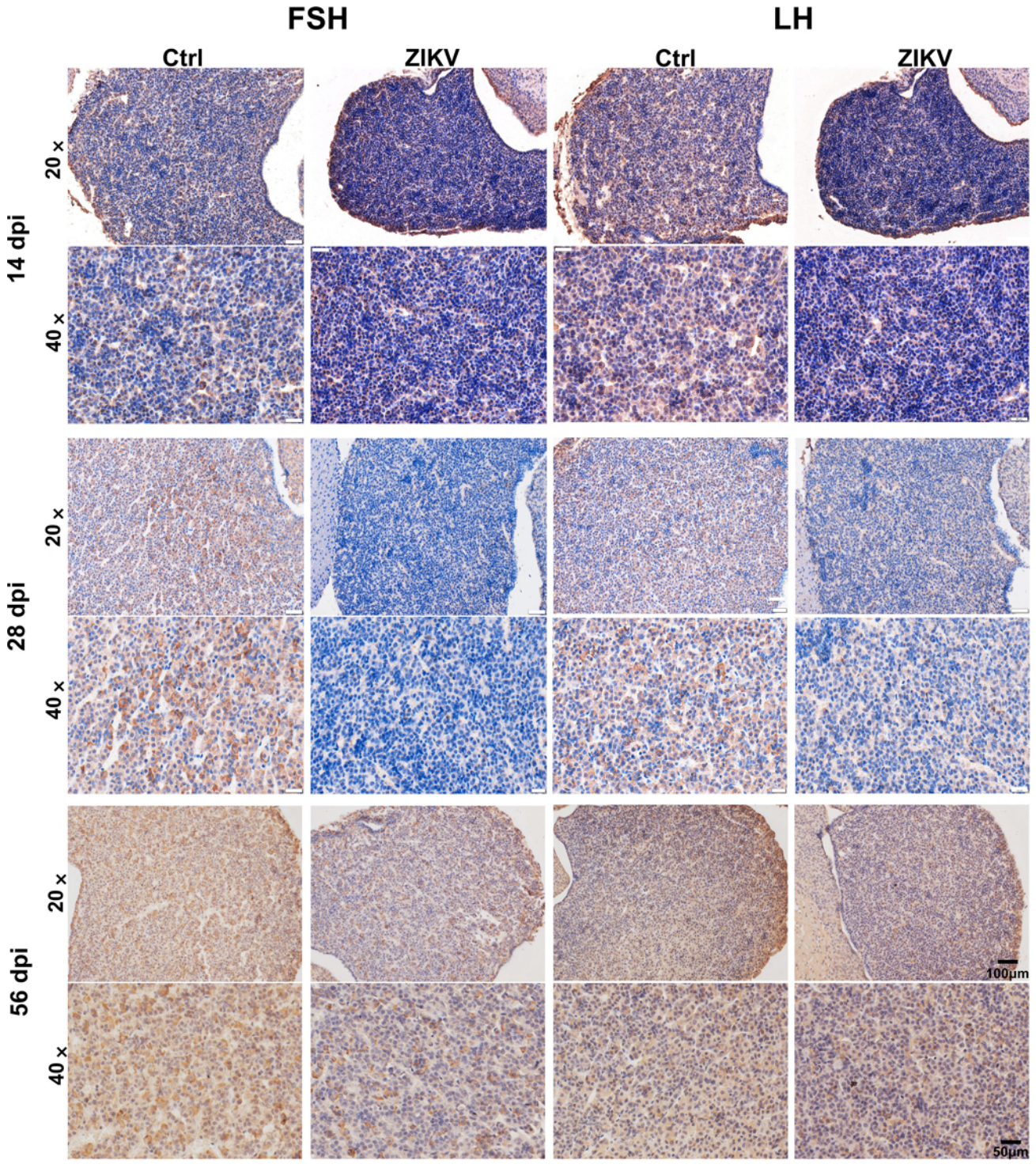

FIG 8 Immunohistochemical staining for FSH and LH in the pituitary of ZIKV-infected and control mice at 14, 28, and 56 dpi.

significantly reduced OXT$^+$ cells at 56 dpi (Fig. 9A and B). The reduced OXT$^+$ cells were also observed in the supraoptic nucleus and paraventricular nucleus of ZIKV-infected mice at 28 and 56 dpi (Fig. 10). No co-staining of ZIKV and OXT was observed (Fig. 10). These results suggested that ZIKV infection reduced oxytocin expressions, which might be associated with abnormal social behavior in mice.

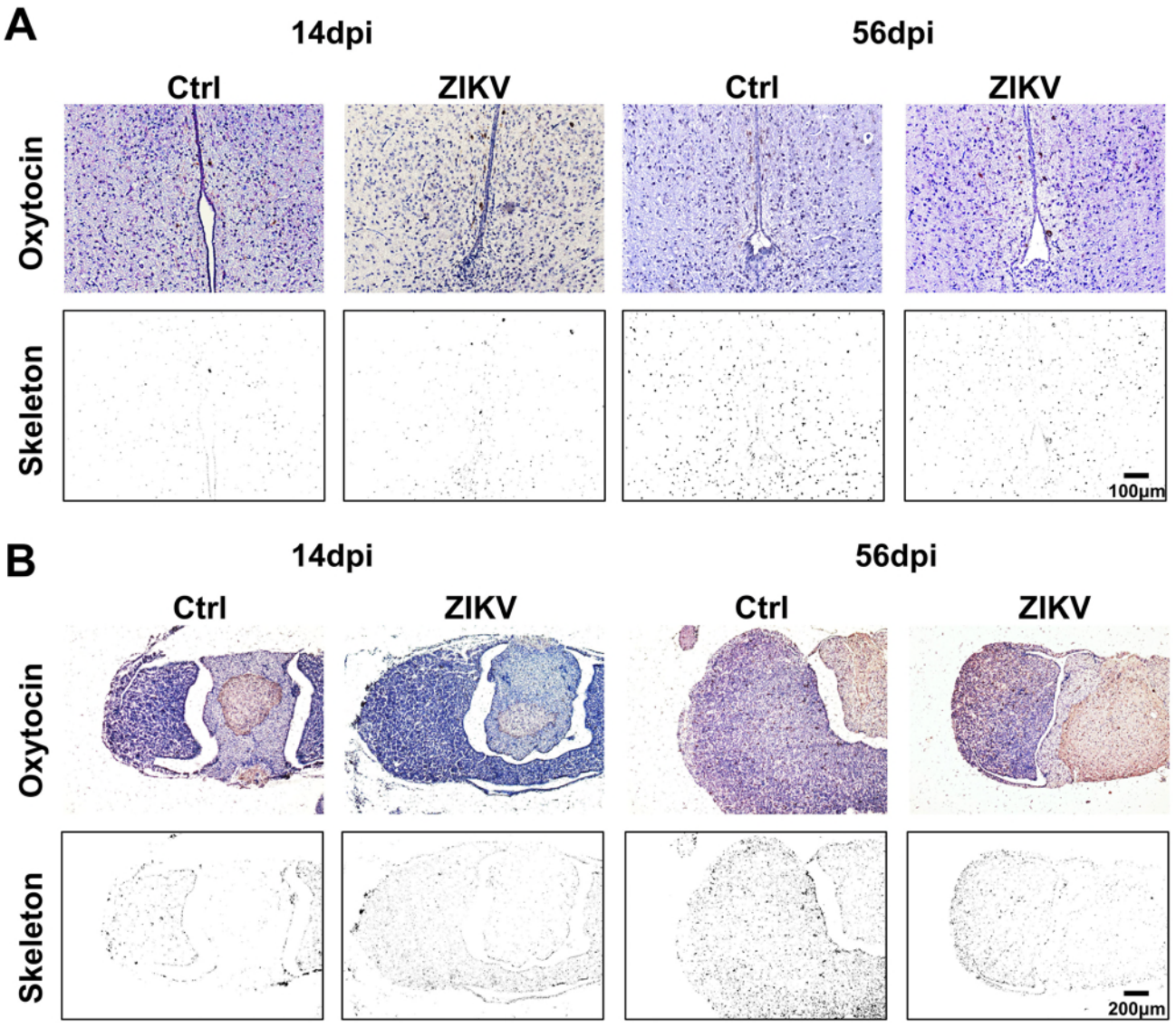

FIG 9 Effects of ZIKV infection on oxytocin production. (A) Immunohistochemical staining for oxytocin in the hypothalamus of ZIKV-infected and control mice at 14 and 56 dpi. Scale bar = 100 μm. (B) Immunohistochemical staining for oxytocin in the pituitary of ZIKV-infected and control mice at 14 and 56 dpi. Scale bar = 200 μm. Skeleton indicates positive staining for oxytocin extracted by skeleton analysis of ImageJ software.

Transcriptome characteristics of hypothalamus and testes in ZIKV-infected mice

To further investigate the effects of ZIKV infection on the hypothalamus, we performed RNA-seq to analyze transcriptome changes in the hypothalamus of mice. Hypothalamus samples were collected from ZIKV-infected and control mice at 10 and 56 dpi. The difference in hypothalamic transcriptome between ZIKV-infected and control mice was remarkable at 10 dpi, and decreased at 56 dpi, albeit still significant (Fig. 11A). We found more differentially expressed genes (DEGs) at 10 dpi (including 1356 up-regulated DEGs and 135 down-regulated DEGs) than at 56 dpi (including 311 up-regulated DEGs and 126 down-regulated DEGs), most of which are related to immune response (Fig. 11B through D). Decreased GnRH and oxytocin expression levels were also observed in ZIKV-infected mice at 10 dpi (Fig. 12A), but there were no significant differences in the expression levels of hormone-related genes (Fig. 12A), which may be due to their low expression levels being overshadowed by differences in immune-related genes. Based on gene set enrichment analysis (GSEA), we found that "Neuropeptide hormone activation,"

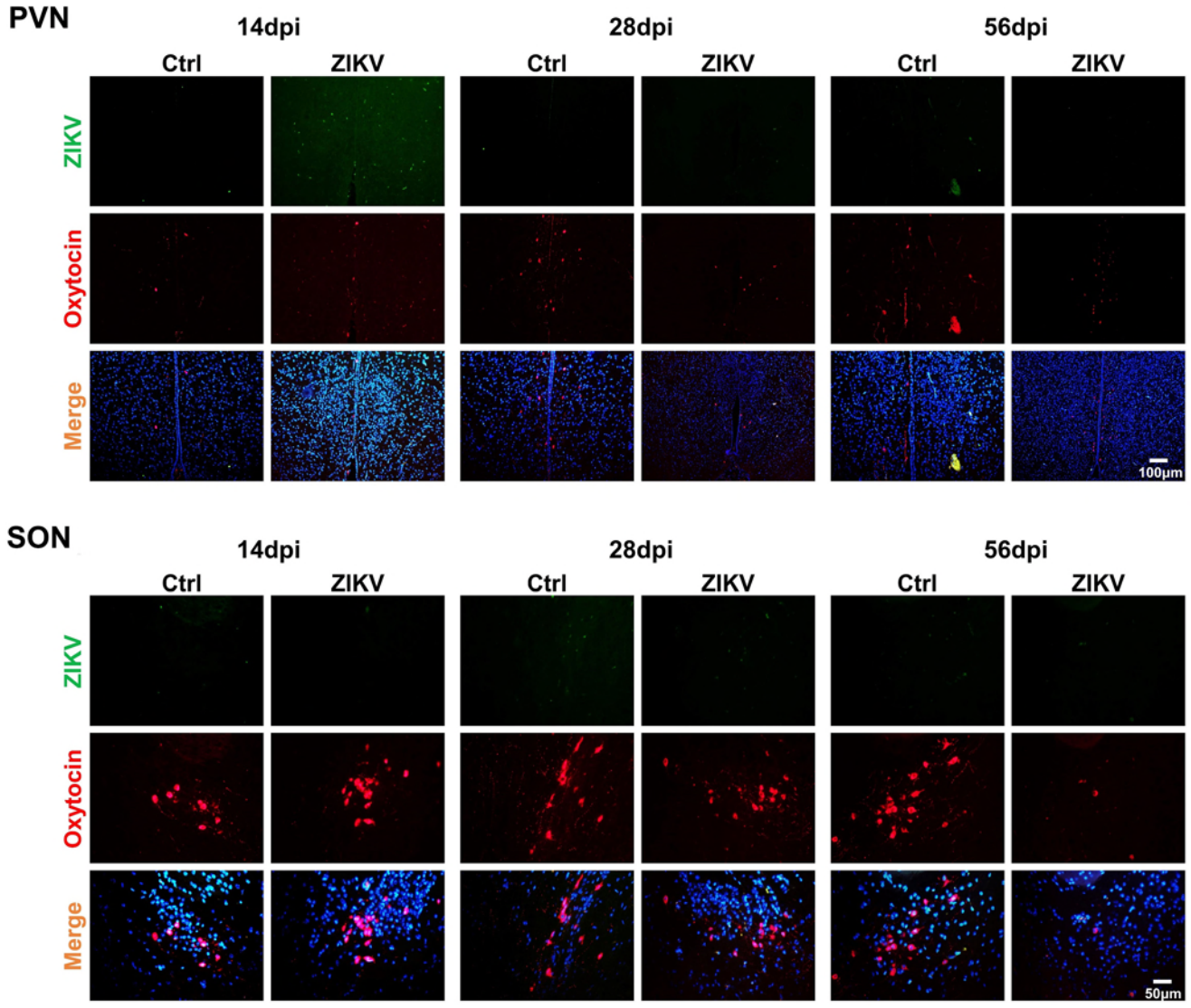

FIG 10 Immunofluorescent staining for ZIKV and oxytocin in the paraventricular nucleus (PVN) and supraoptic nucleus (SON) of ZIKV-infected and control mice at 14, 28, and 56 dpi.

"Endocrine system development," "Neuropeptide binding," and "Positive regulation of hormone biosynthetic process" were inhibited in ZIKV-infected mice (Fig. 12B and C), which may explain the reduced production and secretion of GnRH and oxytocin.

Previous studies have shown that the development of the neuroendocrine system is negatively affected by inflammation (28–30), so we monitor dynamic changes in expression levels of genes related to the inflammatory response (Fig. 13). We observed significantly increased gene expression levels in T cells (e.g., Cd3e, Cd8a, Cd4), NK cells (e.g., Nkg7, Fcgr3, Gzma), and monocytes (e.g., Ccr2, Itgax, Ly6c2) but not B cells and neutrophils in the ZIKV-infected hypothalamus at 10 dpi. The expression levels of genes associated with macrophage and microglia activation were also significantly increased, including Cd68, Cd84, C1qa, C3, Aif1, and H2-D1. In addition, the expression levels of chemokines (e.g., Ccl2, Ccl5, and Ccl12), interferon-stimulated genes (e.g., Isg15, Ifi27l2a, and Irf7), and inflammatory factors (e.g., Ifng, Il1b, Tnf, and Tgfbi) also increased significantly at 10 dpi. Surprisingly, although differences in immune-related genes decreased over time, infiltration of $CD8^+$ T cells, NK cells, and monocytes, activation of macrophages/microglia, and inflammatory responses persisted up to 56 dpi (Fig. 13), which

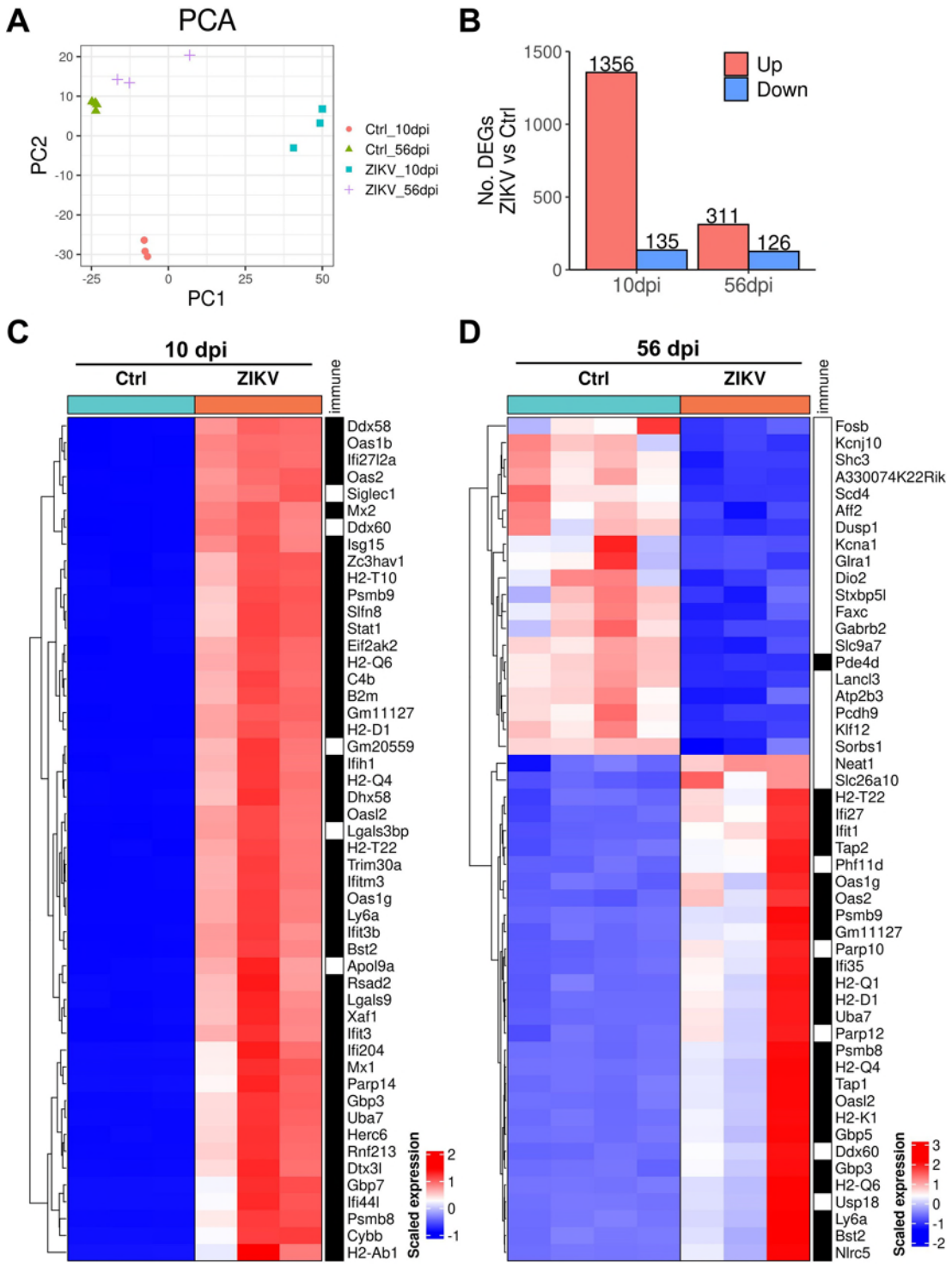

FIG 11 Transcriptome characteristics of the hypothalamus from neonatal ZIKV-infected mice. Hypothalamic samples collected from ZIKV-infected and control mice at 10 and 56 dpi were subjected to RNA-seq. (A) PCA plots of hypothalamic samples were collected from ZIKV-infected and control mice at 10 and 56 dpi. (B) The number of up-regulated and down-regulated DEGs (ZIKV group vs Ctrl group) at 10 and 56 dpi (FDR-adjusted *P*-value < 0.05, |log2 fold change| > 1). (C and D) Heatmaps of differentially expressed genes (Top 50) from the transcriptome of the hypothalamus in ZIKV-infected and control mice at 10 dpi (C) and 56 dpi (D) (FDR-adjusted *P*-value < 0.05, |log2 fold change| > 1). The black blocks in the right annotation indicate genes associated with immune response.

may have had a long-term negative effect on the development of hypothalamic neuroendocrine cells.

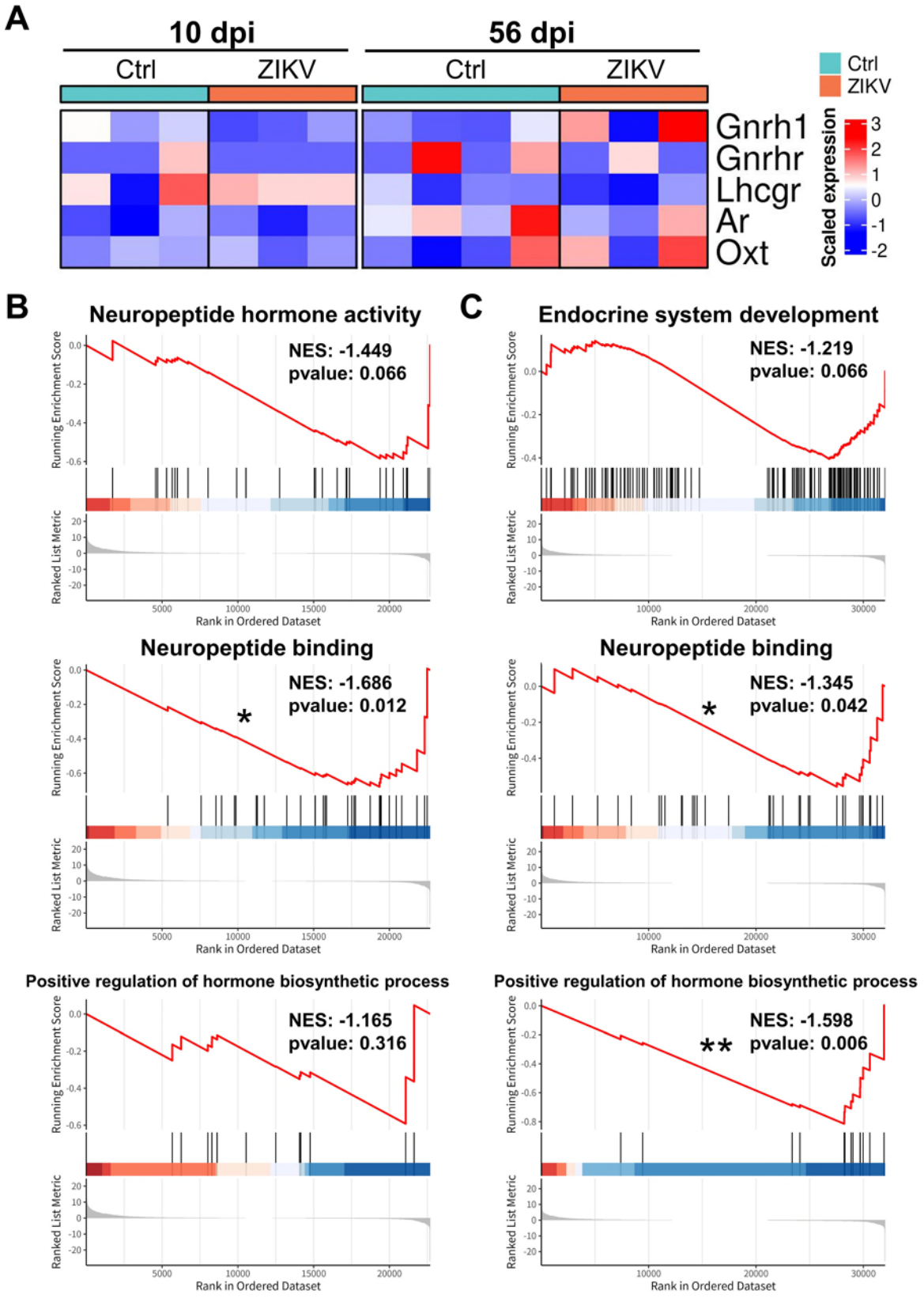

FIG 12 Transcriptome analysis of neuroendocrine genes in the hypothalamus of ZIKV-infected mice. (A) Heatmaps of genes related to the HPG axis from the transcriptome of the hypothalamus in ZIKV-infected and control mice at 10 and 56 dpi. (B and C) GSEA diagrams associated with the neuroendocrine system in the transcriptome of the hypothalamus at 10 dpi (B) and 56 dpi (C) (*$P < 0.05$; **$P < 0.01$; permutation test).

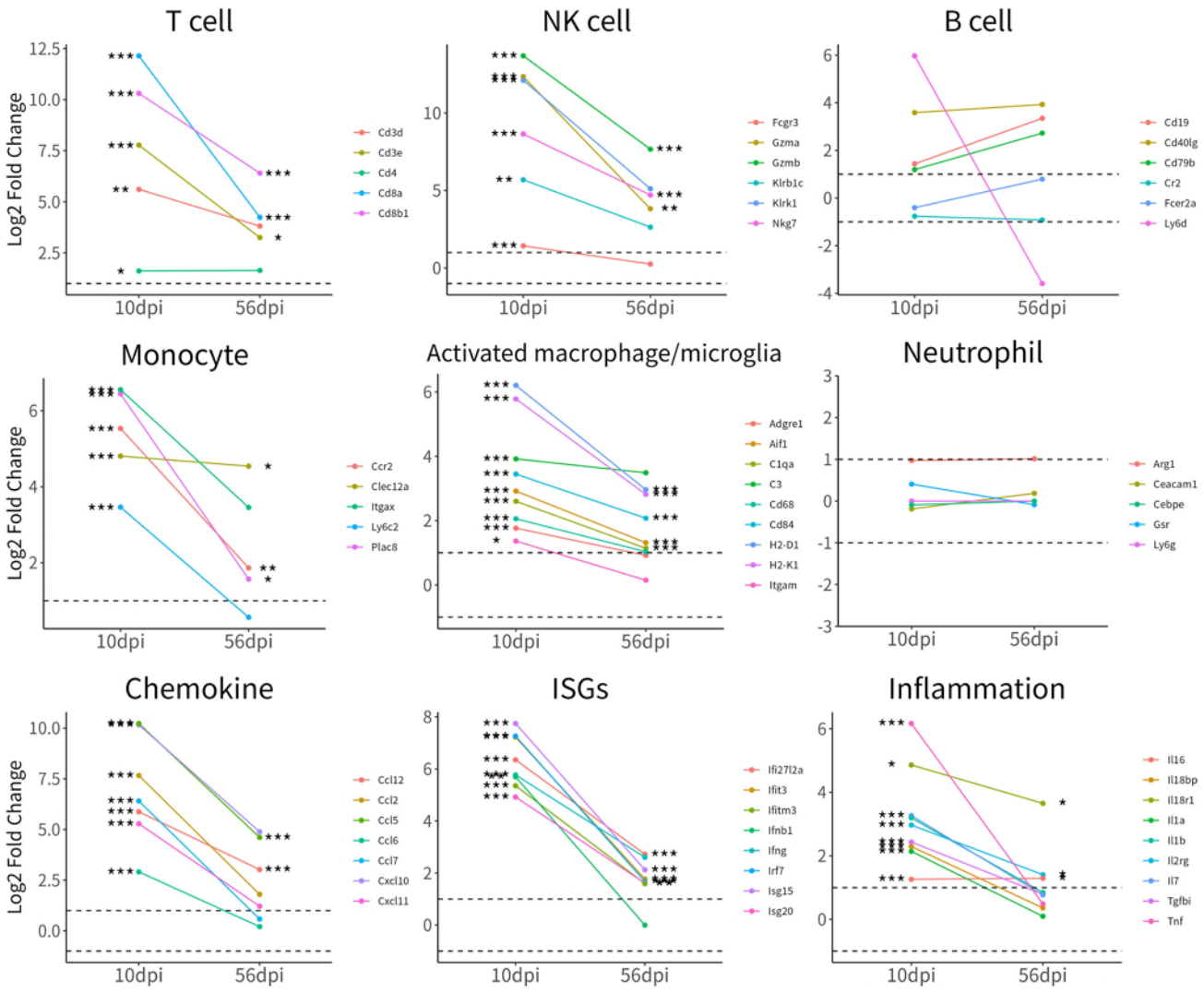

FIG 13 Line graph of T-cell biomarkers, NK cell biomarkers, B-cell biomarkers, monocyte biomarkers, activated macrophage/microglia biomarkers, neutrophil biomarkers, chemokine genes, interferon-stimulated genes (ISGs), and inflammatory genes. Shown are the change of log2 fold change values relative to control mice at 10 and 56 dpi. The dashed lines represent up-regulated and down-regulated gene thresholds (|Log2FC| > 1). The asterisk (*) represents the statistical difference between the ZIKV-infected group and the control group (*P < 0.05; **P < 0.01; ***P < 0.001; Wald test).

Finally, we performed RNA-seq on testes at 56 dpi to follow the long-term consequences of testes from ZIKV-infected mice. ZIKV-infected and control mice had similar testicular transcriptome levels at 56 dpi (Fig. 14A). There were three up-regulated DEGs and 23 down-regulated DEGs in the testes of ZIKV-infected mice (Fig. 14B). Most down-regulated DEGs were related to metabolism, including Zfp46, Arl15, Rps13-ps1, and Rps13-ps2 (Fig. 14C). Lower Cbll1 (encodes the E3 ubiquitin ligase of the E-cadherin complex) expression might reduce the strength of cell adhesion. Higher Mapt expression could promote microtubule assembly and stability (31). In addition, ZIKV-infected testes showed no abnormal immune and reproductive genes. Generally, ZIKV-infected mice had nearly normal transcriptome in the testis at 56 dpi, which is distinct from significant transcriptome changes in the hypothalamus.

Taken together, ZIKV could damage the hypothalamus of mice for a longer time, and immune responses persisted even up to 56 dpi. By contrast, ZIKV just transiently affected the testes of ZIKV-infected mice and did not disturb expressions of its spermatogenic genes.

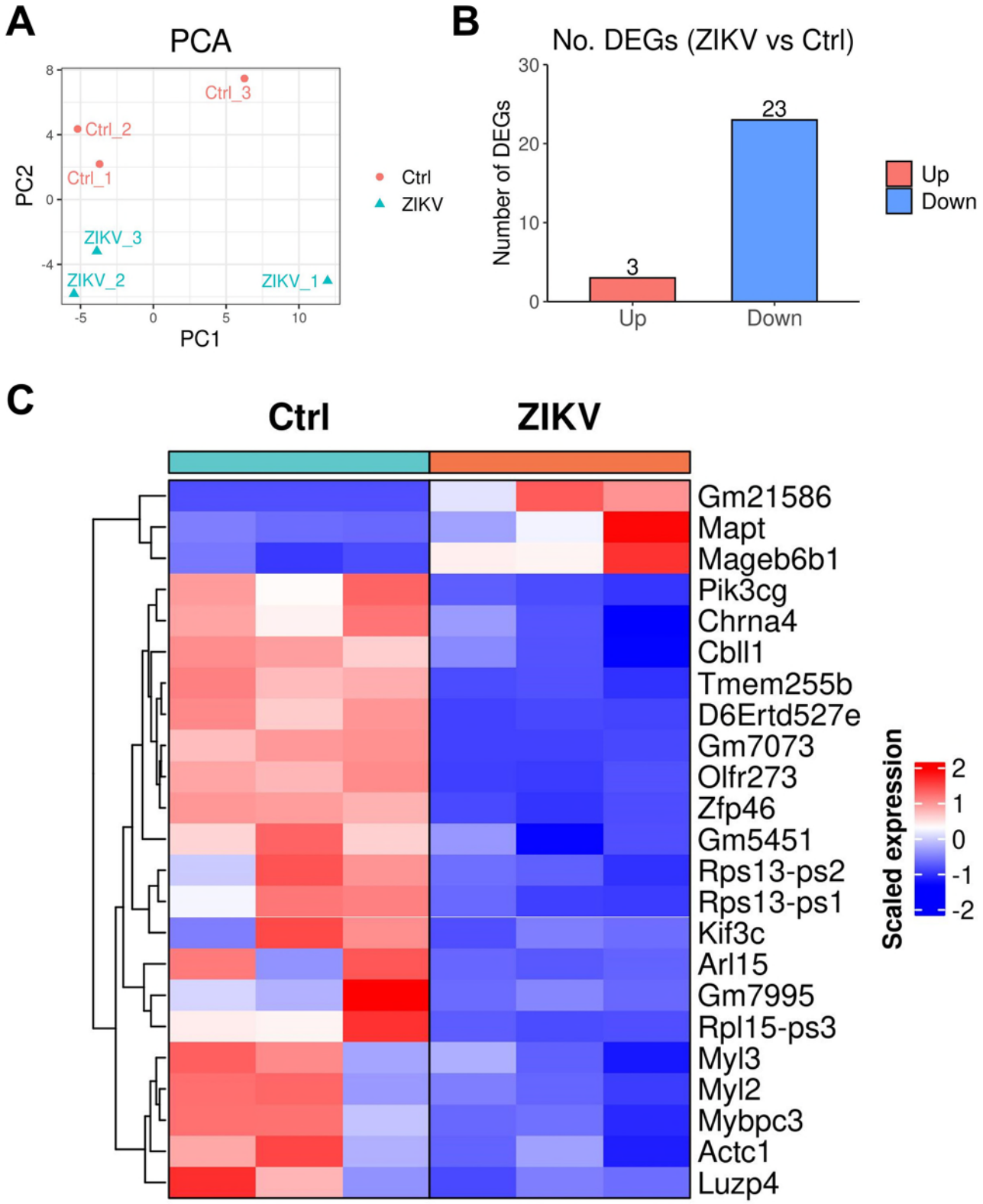

FIG 14 Transcriptome characteristics of testis from neonatal ZIKV-infected mice. Testis samples collected from ZIKV-infected and control mice at 56 dpi were performed by RNA-seq. (A) PCA plots of testis samples collected from ZIKV-infected and control mice at 56 dpi. (B) The number of up-regulated and down-regulated DEGs (ZIKV group vs Ctrl group) at 56 dpi (FDR-adjusted *P*-value < 0.05, |log2 fold change| > 1). (C) Heatmaps of all differentially expressed genes from the transcriptome of testis in ZIKV-infected and control mice.

DISCUSSION

Newborns exposed to ZIKV have received global attention because of their developmental complications, including delays in cognitive, language, and motor development (12–15) as well as cryptorchidism (16, 17). However, the impacts of ZIKV infection on the reproductive health of these children remain unclear. In the current study, using a mouse model, we demonstrated that long-term hormone deficiencies of the HPG axis caused by postnatal ZIKV infection resulted in not only decreased sperm quality and quantity but also abnormal behavior, ultimately leading to diminished fertility.

In this study, male BALB/c suckling mice were inoculated with ZIKV at postnatal day 2, which is equivalent to the neonatal infection during the third trimester (19, 20). This animal model was widely used to study developmental delays of newborns exposed to ZIKV (18, 20). For example, Zhao et al. (20) found that postnatal ZIKV-infected mice had neurological deficits in social interaction, learning, and memory, which was consistent with neurodevelopmental deficits observed in children perinatally exposed to ZIKV in Brazil (12). In comparison to immunodeficient mice (e.g., *Ifnar1*$^{-/-}$ mouse), this neonatal mouse model better mimics human diseases, suggesting that it may be more suitable for studying congenital ZIKV syndrome.

Using the neonatal mouse model, we observed brain atrophy, abnormal social behaviors, and stereotypic behaviors in ZIKV-infected mice, which were consistent with the observations in several ZIKV-infected animal models reported previously (20, 32, 33). Previous studies have focused primarily on the cortex and the visual system and found that all kinds of central nervous system (CNS) cells were susceptible to ZIKV infection, exhibiting cell death and decreased neurogenesis (34–36), which were thought to be a major contributor of various neurodevelopmental complications in ZIKV infection. However, the effects of ZIKV infection on the hypothalamus have hardly been studied. In this study, we detected the presence of ZIKV in the hypothalamus, which was consistent with our previous study (18, 37). As the center of the neuroendocrine system, the hypothalamus can release hormones to regulate various important physiological processes, such as GnRH regulating reproductive development via the HPG axis (38) and oxytocin regulating social behaviors (26, 27). Both GnRH and oxytocin secreted by the hypothalamus were significantly reduced in ZIKV-infected mice, which was highly correlated with persistent damage of ZIKV infection. We speculated that the long-term decreased hormones secreted by the hypothalamus contribute to the delayed testicular development, abnormal sperm, abnormal social behaviors, and decreased fertility, which for the first time linked the hypothalamus to the reproductive system and social behaviors after ZIKV infection.

GnRH can directly act on anterior pituitary cells to regulate releases of FSH and LH (39, 40). In this study, serum FSH and LH concentrations had a long-term decrease, albeit transiently increased within the first week after infection, which was possibly attributed to the break of negative feedback balance of the HPG axis caused by persistent GnRH reduction. FSH can promote the proliferation and development of spermatogenic cells and Sertoli cells (41, 42). In this study, the lower serum FSH concentration was possibly the reason for reversible developmental delays of spermatogenic cells and Sertoli cells in the testes of ZIKV-infected mice. In addition, spermatogenesis depends primarily on the stimulation of FSH, LH, and testosterone (41, 43, 44). FSH can promote spermatogenesis directly by stimulating spermatogenic cells (41, 43, 44). LH deficiency could result in azoospermia, as revealed by Abel et al. (45). Consequently, persistent lower FSH and LH levels in the study most likely led to decreases in sperm quantity and quality of mice, which resulted in decreased fertility and decreased offspring quality.

In previous studies, ZIKV infection can cause severe damage to testicular morphology and massive inflammatory cell infiltration in C57BL/6 mice treated with anti-Ifnar1 blocking monoclonal antibody (24) or Ifnar1$^{-/-}$ mice (22, 23), and ZIKV infection was thought a major contributor of the testicular damage. In the current study, ZIKV was detected in only 40% (2/5) of BALB/c mouse testes, and there was no serious damage and inflammatory cell infiltration, which was distinct from the immunodeficient mice

mentioned above. Considering the low infection rate of testes but sperm abnormalities when ZIKV was eliminated, we speculated that testicular developmental delays and oligospermia observed in BALB/c mice were primarily attributed to hormone deficiencies of the HPG axis rather than the direct attack of ZIKV to testes or the immune injury.

The diminished fertility may be associated with many factors in mice. On the one hand, hormone disorders of the HPG axis led to decreases in sperm quantity and quality in ZIKV-infected mice, which directly affects the fertility rate and quality of offspring mice. On the other hand, the decreased preference for females and stereotyped behaviors observed in ZIKV-infected mice reduced their mating behavior, which might be another important cause for the prolonged time to delivery. Therefore, in future experiments, administering GnRH or oxytocin may be a way to improve fertility by regulating hormone levels of the HPG axis or mating behavior.

Healthy male mammals usually experience several physiological testosterone elevations: the first at embryonic day 13 of mice or the 7th week of pregnancy in humans, the second in neonates, and the third at puberty (25). After a neonatal testosterone surge, testosterone drops to a low level until puberty (25). In this study, however, ZIKV-infected mice did not show a physiological decrease in serum testosterone from birth till adulthood, the pathogenesis of which remains unclear and may be related to the blocked consumption of testosterone. As a protective hormone against ZIKV infection (46), whether disordered testosterone level in postnatal ZIKV-infected mice affects disease progression needs to be further studied.

In summary, we comprehensively clarified the effects of postnatal ZIKV infection on fertility from multiple perspectives including the HPG axis, testis, sperm, and abnormal behaviors, revealing that postnatal ZIKV infection caused long-term hormone deficiencies and diminished fertility in mice. Although the extent to which these observations in mice translate to humans remains unclear, these findings did suggest that the reproductive health and hormone levels of ZIKV-exposed children should receive more attention to improve their living quality.

MATERIALS AND METHODS

Cells and virus

C6/36 cells were cultured in RPMI 1640 medium (Gibco, USA) with 10% fetal bovine serum (FBS, PAN, Germany) and maintained at 28°C. Vero cells were cultured in minimum essential medium (MEM, Gibco, USA) with 5% FBS and maintained at 37°C. ZIKV (strain SMGC-1, Asian lineage, GenBank accession number: KX266255,) was propagated in C6/36 cells and titrated on Vero cells under overlay medium containing 1.2% methylcellulose by plaque assay. Stocks were stored at 80°C until use.

Mouse

Pregnant BALB/c mice from the Beijing Vital River Laboratory Animal Technology Co., Ltd. (Beijing, China) were bred and maintained under a specific pathogen-free animal facility at Capital Medical University.

Mouse experiments

Mouse pups at postnatal day 2 were inoculated from the brain λ point with 100 plaque-forming units of ZIKV or an equal volume of phosphate-buffered saline (PBS). The body weight and survival rate of mice were recorded for 56 days. Hypothalamus, pituitary, and testis were collected at 7, 10, 14, 21, 28, 42, and 56 dpi to study morphology, ZIKV RNA, and transcriptome. To determine the effects of ZIKV infection on fertility, ZIKV-infected and control male mice were mated with healthy age-matched female mice in a ratio of 1:2 when they were 6 or 8 weeks old. The 6-week mating experiment and the 8-week mating experiment were independent experiments in different batches. The pregnancy

rate and time from being co-caged to delivery were observed for 50 days. The body weight and sex ratio of offspring mice were recorded at postnatal days 0 and 28.

ZIKV RNA quantification and GnRH mRNA relative quantification

Hypothalamus, pituitary, and testis were harvested from ZIKV-infected and control mice at different time points as indicated. RNA was extracted from tissue lysates by Trizol (Transgen China, ET101-01) according to the manufacturer's protocol. Real-time quantitative PCR (RT-qPCR) was performed as previously reported (18) by Quant One Step RT-qPCR (Tiangen, China) on a 7500 Real-Time PCR System (Applied Biosystems, USA). ZIKV RNA copies of samples were quantified as the copy number per microgram of total RNA by the standard curve method. ZIKV RNA copies transcribed *in vitro* were quantified and used as a standard template to establish the standard curve. Relative quantification of GnRH mRNA was determined by the $2^{-\Delta\Delta Ct}$ method. The primer sequences were as follows: ZIKV forward: 5′-TCAGACTGCGACAGTTCGAGT-3′; ZIKV reverse: 5′-GCATATTGACAATCCGGAAT-3′; GAPDH forward: 5′-GCATTGTGGAAGGGC-TCA-3′; GAPDH reverse: 5′-ACCAGTGGATGCAGGGAT-3′; GnRH forward: 5′-AGCACTGGT-CCTATGGGTTG-3′; GnRH reverse: 5′-GGGGTTCTGCCATTTGATCCA-3′ (47).

ELISA

The serum GnRH, FSH, LH, and testosterone concentrations in mice were quantified by ELISA, according to the manufacturer's instructions. ELISA reagents of GnRH, FSH, and LH were purchased from Cloud-Clone (mouse GnRH, FSH, and LH ELISA Kits, Cloud-Clone, China). Briefly, 100 µL of standard dilution or serum dilution was added into each well, then the plate was incubated for 1 h at 37°C. Subsequently, 50 µL of Detection Reagent A was added and the plate was incubated for 1 h at 37°C. After washing, 50 µL of Detection Reagent B was added and the plate was incubated for 30 min. Finally, 90 µL of Substrate Solution was added and the plate was incubated at 37°C for 15 min, followed by the addition of 50 µL of Stop Solution. The absorbance was measured at 450 nm in a Multiskan spectrum 1500 (Thermo, USA). ELISA reagents of testosterone were purchased from Enzo Life Sciences (Testosterone ELISA kit, Enzo Life Sciences, USA). Briefly, 100 µL of standard dilution or serum dilution and 50 µL of yellow Antibody were added into each well, then the plate was incubated for 1 h at 500 rpm. Subsequently, 50 µL of blue Conjugate was added and the plate was incubated for 1 h at 500 rpm. After washing, 200 µL of the pNpp Substrate solution was added, and the plate was incubated for 1 h at 37°C. Finally, 50 µL of Stop Solution was added. The absorbance was measured at 405 nm in a Multiskan spectrum 1500 (Thermo, USA).

Immunohistochemistry staining

To assay hormone expressions in the hypothalamus and pituitary, tissues were fixed in 4% paraformaldehyde solution overnight, then dehydrated, and paraffin-embedded. Tissue sections were incubated with rabbit polyclonal anti-GnRH (PAA843Mu01, Cloud-Clone, China), anti-FSH (PAA830Mu01, Cloud-Clone, China), anti-LH (PAA441Ra01, Cloud-Clone, China), and anti-Oxytocin (ab212193, Abcam) overnight. After washing, the slides were stained with a secondary HRP-conjugated goat anti-rabbit antibody (Zhongshan Golden Bridge Bio Co., Ltd., China) for 1 h. The reaction was visualized by the addition of 3,30-diaminobenzidine (DAB) as a chromogen and then stopped by removing the DAB and then it was washed with running water. Images were captured with the Olympus microscope (IX71, Olympus, Japan). Skeleton analysis was performed using ImageJ.

Hematoxylin and eosin staining

To investigate pathological changes in ZIKV-infected testes, testicular sections were subjected to HE staining. Testicular sections were immersed into xylene and alcohol,

then stained with hematoxylin for 12 min. After being stained with eosin for 20 min and re-immersed in alcohol and xylene, sections were mounted by synthetic resin.

Immunofluorescence staining

Tissue sections were incubated with mouse anti-ZIKV NS1 monoclonal antibody (1:500, GT5212, Invitrogen), mouse anti-DDX4 antibody (1:400, ab27591, Abcam), rabbit anti-SOX9 antibody (1:400, AB5535, Millipore), and rabbit anti-Oxytocin antibody (1:400, ab212193, Abcam) as the primary antibody at 4°C overnight, and then incubated with Alexa Fluor 488 goat anti-mouse IgG (1:1000, A21202, Invitrogen, USA) or Alexa Fluor 594 donkey anti-rabbit IgG (1:1000, A21207, Invitrogen, USA) at 37°C for 1 h. All images were captured with laser confocal scanning microscopy (Leica TCS SP5).

Papanicolaou staining of sperm

Epididymides of ZIKV-infected or control mice at 56 dpi were collected. After being clipped on the tail, epididymides were placed in PBS and incubated at 37°C for 20 min. The 50 µL of supernatant was placed on dry glass slides. After air-drying naturally, slides were first immersed in 95% ethanol for 10 min; then sequentially immersed in 85% ethanol, 80% ethanol, 70% ethanol, and purified water; and stained with hematoxylin. After differentiation by hydrochloric acid ethanol, the slides were sequentially stained with G-6 orange and EA-50. After being re-immersed in alcohol and xylene, slides were mounted by synthetic resin.

Library preparation and RNA sequencing

RNA sequencing of the hypothalamus and testes harvested from ZIKV-infected or control mice at 10 and 56 dpi was commercially conducted (LC-Bio Technology Co., Ltd., Hangzhou, China). Three to four individuals were in each group. In brief, after extraction of total RNA (Trizol reagent, ThermoFisher, 15596018), mRNA was purified by Dynabeads Oligo (dT) (Thermo Fisher, CA, USA). The mRNA was fragmented by Magnesium RNA Fragmentation Module (NEB, cat.e6150, USA) to create cDNA libraries. A real-time PCR system was used to quantify and qualify the sample libraries. Finally, the cDNA libraries were sequenced using Illumina Novaseq 6000 (Illumina, Inc., USA).

Bioinformatics analysis

To get high-quality clean reads, we further filtered reads using Cutadapt v1.9. For reads mapping, the reference genome (GRCm39) was downloaded from the Ensembl website (ftp://ftp.ensembl.org/pub/current_gtf). We aligned reads of all samples to the GRCm39 reference genome using HISAT2 v2.2.1 (48). StringTie and Ballgown were used to estimate the expression levels of all genes and transcripts and calculate the FPKM (fragment per kilobase of transcript per million mapped reads) value (49). Differentially expressed gene analysis between two groups and principal component analysis (PCA) were performed by DESeq2 v1.34.0 (50). Genes with adjusted *P*-value < 0.05 and |Log2 fold change| ≥ 1 were considered as DEGs. Gene ontology (GO) enrichment analysis, KEGG pathways enrichment analysis, and GSEA were conducted by clusterProfiler v4.2.2 (51). Graphics drawing was conducted by the ggplot2 v3.4.0 and ComplexHeatmap v2.13.1.

Three-chamber task

The social behavior and social novelty preference of mice were examined by a three-chamber task (52). The apparatus which consisted of a clear rectangular plastic box (75 × 30 cm) was divided into three equal compartments (25 × 30 cm) by plastic dividers with an opening. Test mice were allowed to habituate in the middle chamber for 5 min when openings were closed by removable doors. The doors were then opened and mice were allowed to explore the entire box for 5 min. The social test consisted of 5

min where one of the side chambers was randomly selected as the social side and the other as the non-social side. In the social chamber, an 8-week-old male mouse (Stranger 1) was placed under a wire cup. The non-social side consisted of an empty cup. The social novelty preference test consisted of 5 min where the previous non-social side was put into another 8-week-old male mouse (Stranger 2) under a wire cup. Mice were videotaped during the entire session. The index of social novelty preference is calculated by (Stranger 2 time – Stranger 1 time) / (Stranger 1 time +Stranger 2 time) ×100%.

The sexual preference of male mice was examined by a three-chamber task. The apparatus is consistent with the above experiment. The sexual preference test consisted of 5 min where one of the side chambers was the female mouse side and the other was the male mouse side. A new female mouse (8 weeks old) and a new male mouse (8 weeks old) were placed in the side chambers under wire cups, respectively. Mice were videotaped during the entire session.

Open field test

The open field test was carried out to evaluate the motor ability and autonomous exploration (53). The apparatus is a well-lit transparent square cage (50 × 50 cm) equipped with a black floor. Each mouse was placed in the corner of the cage. The total distance traveled (m), total freezing episodes, total time freezing(s), time spent in the center zone (40 × 40 cm), time spent in the limb zone, and maximum speed (m/s) were measured for 5 min by the ANY-maze system.

Statistical analysis

R v4.1.2 and GraphPad Prism v7.0 were used for statistical analysis. The quantitative data between two groups with normal distributions were analyzed by Student's *t*-test. All results in this study were presented as the mean ± standard deviation (SD) from at least three repeats. $P < 0.05$ (*), $P < 0.01$ (**), and $P < 0.001$ (***) was considered significant difference between the two groups.

ACKNOWLEDGMENTS

This work was supported by the National Key Research and Development Program of China (2021YFC2300202); the National Natural Science Foundation of China (U1902210, 81871641, 81972979, 82172266, and 81902048); the Support Project of High-level Teachers in Beijing Municipal Universities in the Period of 13th Five-year Plan (IDHT20190510); and the Beijing Key Laboratory of Emerging Infectious Diseases (DTKF202103).

The authors declare no conflict of interest.

AUTHOR AFFILIATIONS

[1]Department of Microbiology, School of Basic Medical Sciences, Capital Medical University, Beijing, China
[2]Department of Neurosurgery, Capital Medical University Sanbo Brain Hospital, Beijing, China
[3]Center of Epilepsy, Beijing Institute for Brain Disorders, Beijing, China

AUTHOR ORCIDs

Li-Bo Liu http://orcid.org/0000-0002-6369-9459
Jing An http://orcid.org/0000-0002-2567-0380

FUNDING

Funder	Grant(s)	Author(s)
MOST | National Key Research and Development Program of China (NKPs)	2021YFC2300202	Jing An
MOST | National Natural Science Foundation of China (NSFC)	U1902210	Jing An
MOST | National Natural Science Foundation of China (NSFC)	81871641	Pei-Gang Wang
MOST | National Natural Science Foundation of China (NSFC)	81972979	Jing An
MOST | National Natural Science Foundation of China (NSFC)	82172266	Pei-Gang Wang

AUTHOR CONTRIBUTIONS

Li-Bo Liu, Conceptualization, Data curation, Formal analysis, Investigation, Methodology, Software, Validation, Visualization, Writing – original draft, Writing – review and editing | Wei Yang, Conceptualization, Investigation, Methodology, Software, Visualization, Writing – review and editing | Jia-Tong Chang, Formal analysis, Investigation, Software | Dong-Ying Fan, Data curation, Supervision | Yan-Hua Wu, Conceptualization, Supervision | Pei-Gang Wang, Conceptualization, Methodology, Project administration, Resources, Supervision, Writing – review and editing | Jing An, Conceptualization, Data curation, Funding acquisition, Methodology, Project administration, Resources, Supervision, Writing – review and editing

DATA AVAILABILITY

The raw sequencing data were deposited at the NCBI Sequence Read Archive (SRA) under the BioProject accession number PRJNA994603.

ETHICS APPROVAL

All animal experiments were approved and conducted following the guidelines established by the Institutional Animal Care and the Animal Ethics Committees of Capital Medical University (Approval number: AEEI-2015–048).

REFERENCES

1. Pierson TC, Diamond MS. 2020. The continued threat of emerging flaviviruses. Nat Microbiol 5:796–812. https://doi.org/10.1038/s41564-020-0714-0
2. Pierson TC, Diamond MS. 2018. The emergence of Zika virus and its new clinical syndromes. Nature 560:573–581. https://doi.org/10.1038/s41586-018-0446-y
3. Wikan N, Smith DR. 2016. Zika virus: history of a newly emerging arbovirus. Lancet Infect Dis 16:e119–e126. https://doi.org/10.1016/S1473-3099(16)30010-X
4. Lessler J, Chaisson LH, Kucirka LM, Bi Q, Grantz K, Salje H, Carcelen AC, Ott CT, Sheffield JS, Ferguson NM, Cummings DAT, Metcalf CJE, Rodriguez-Barraquer I. 2016. Assessing the global threat from Zika virus. Science 353:aaf8160. https://doi.org/10.1126/science.aaf8160
5. Liu ZY, Shi WF, Qin CF. 2019. The evolution of Zika virus from Asia to the Americas. Nat Rev Microbiol 17:131–139. https://doi.org/10.1038/s41579-018-0134-9
6. Musso D, Ko AI, Baud D. 2019. Zika virus infection - after the pandemic. N Engl J Med 381:1444–1457. https://doi.org/10.1056/NEJMra1808246
7. Liu J, Liu Y, Shan C, Nunes BTD, Yun R, Haller SL, Rafael GH, Azar SR, Andersen CR, Plante K, Vasilakis N, Shi P-Y, Weaver SC. 2021. Role of mutational reversions and fitness restoration in Zika virus spread to the Americas. Nat Commun 12:595. https://doi.org/10.1038/s41467-020-20747-3
8. Moore CA, Staples JE, Dobyns WB, Pessoa A, Ventura CV, Fonseca E da, Ribeiro EM, Ventura LO, Neto NN, Arena JF, Rasmussen SA. 2017. Characterizing the pattern of anomalies in congenital Zika syndrome for pediatric Clinicians. JAMA Pediatr 171:288–295. https://doi.org/10.1001/jamapediatrics.2016.3982
9. Miner JJ, Diamond MS. 2017. Zika virus pathogenesis and tissue tropism. Cell Host Microbe 21:134–142. https://doi.org/10.1016/j.chom.2017.01.004
10. Li C, Xu D, Ye Q, Hong S, Jiang Y, Liu X, Zhang N, Shi L, Qin CF, Xu Z. 2016. Zika virus disrupts neural progenitor development and leads to microcephaly in mice. Cell Stem Cell 19:120–126. https://doi.org/10.1016/j.stem.2016.04.017
11. de Carvalho NS, de Carvalho BF, Dóris B, Silverio Biscaia E, Arias Fugaça C, de Noronha L. 2017. Zika virus and pregnancy: an overview. Am J Reprod Immunol 77. https://doi.org/10.1111/aji.12616
12. Nielsen-Saines K, Brasil P, Kerin T, Vasconcelos Z, Gabaglia CR, Damasceno L, Pone M, Abreu de Carvalho LM, Pone SM, Zin AA, Tsui I, Salles TRS, da Cunha DC, Costa RP, Malacarne J, Reis AB, Hasue RH, Aizawa CYP, Genovesi FF, Einspieler C, Marschik PB, Pereira JP, Gaw SL, Adachi K, Cherry JD, Xu Z, Cheng G, Moreira ME. 2019. Delayed childhood neurodevelopment and neurosensory alterations in the second year of

life in a prospective cohort of ZIKV-exposed children. Nat Med 25:1213–1217. https://doi.org/10.1038/s41591-019-0496-1
13. Barros Faiçal AV, de Oliveira JMGC, Andrade NC, Lucena R, Acosta AX, de Siqueira IC. 2020. Socioemotional status of children with uterine exposure to the Zika virus. Pediatr Neurol 103:86–88. https://doi.org/10.1016/j.pediatrneurol.2019.07.020
14. Faiçal AV, de Oliveira JC, Oliveira JVV, de Almeida BL, Agra IA, Alcantara LCJ, Acosta AX, de Siqueira IC. 2019. Neurodevelopmental delay in normocephalic children with in utero exposure to Zika virus. BMJ Paediatr Open 3:e000486. https://doi.org/10.1136/bmjpo-2019-000486
15. Soares F, Abranches AD, Villela L, Lara S, Araújo D, Nehab S, Silva L, Amaral Y, Junior SCG, Pone S, Lobkowicz L, Clemente NS, Brasil P, Nielsen-Saines K, Pone M, Brickley E, Moreira ME. 2019. Zika virus infection in pregnancy and infant growth, body composition in the first three months of life: a cohort study. Sci Rep 9:19198. https://doi.org/10.1038/s41598-019-55598-6
16. de Vasconcelos RAL, Ximenes RAA, Calado AA, Martelli CMT, Gonçalves AV, Brickley EB, de Araújo TVB, Rocha MAW, Miranda-Filho D de B. 2020. Surgical findings in cryptorchidism in children with Zika-related microcephaly: a case series. BMC Urol 20:186. https://doi.org/10.1186/s12894-020-00721-3
17. de Vasconcelos RAL, Ximenes RAA, Calado AA, Martelli CMT, Gonçalves AV, Brickley EB, de Araújo TVB, Wanderley Rocha MA, Miranda-Filho D de B. 2020. Cryptorchidism in children with Zika-related microcephaly. Am J Trop Med Hyg 102:982–984. https://doi.org/10.4269/ajtmh.19-0753
18. Wu YH, Cui XY, Yang W, Fan DY, Liu D, Wang PG, An J. 2018. Zika virus infection in hypothalamus causes hormone deficiencies and leads to irreversible growth delay and memory impairment in mice. Cell Rep 25:1537–1547. https://doi.org/10.1016/j.celrep.2018.10.025
19. Clancy B, Finlay BL, Darlington RB, Anand KJS. 2007. Extrapolating brain development from experimental species to humans. Neurotoxicology 28:931–937. https://doi.org/10.1016/j.neuro.2007.01.014
20. Zhao Z, Shang Z, Vasconcelos Z, Li C, Jiang Y, Zu S, Zhang J, Wang F, Yao L, Jung JU, Brasil P, Moreira ME, Qin C, Kerin T, Nielsen - Saines K, Cheng G, Zhang X, Xu Z. 2020. Zika virus infection leads to variable defects in multiple neurological functions and behaviors in mice and children. Adv Sci 7:1901996. https://doi.org/10.1002/advs.201901996
21. Mead PS, Duggal NK, Hook SA, Delorey M, Fischer M, Olzenak McGuire D, Becksted H, Max RJ, Anishchenko M, Schwartz AM, Tzeng W-P, Nelson CA, McDonald EM, Brooks JT, Brault AC, Hinckley AF. 2018. Zika virus shedding in semen of symptomatic infected men. N Engl J Med 378:1377–1385. https://doi.org/10.1056/NEJMoa1711038
22. Yang W, Wu Y-H, Liu S-Q, Sheng Z-Y, Zhen Z-D, Gao R-Q, Cui X-Y, Fan D-Y, Qin Z-H, Zheng A-H, Wang P-G, An J, Suthar M. 2020. S100A4+ macrophages facilitate Zika virus invasion and persistence in the seminiferous tubules via interferon-gamma mediation. PLoS Pathog 16:e1009019. https://doi.org/10.1371/journal.ppat.1009019
23. Lazear HM, Govero J, Smith AM, Platt DJ, Fernandez E, Miner JJ, Diamond MS. 2016. A mouse model of Zika virus pathogenesis. Cell Host Microbe 19:720–730. https://doi.org/10.1016/j.chom.2016.03.010
24. Govero J, Esakky P, Scheaffer SM, Fernandez E, Drury A, Platt DJ, Gorman MJ, Richner JM, Caine EA, Salazar V, Moley KH, Diamond MS. 2016. Zika virus infection damages the testes in mice. Nature 540:438–442. https://doi.org/10.1038/nature20556
25. Clarkson J, Herbison AE. 2016. Hypothalamic control of the male neonatal testosterone surge. Philos Trans R Soc Lond B Biol Sci 371:20150115. https://doi.org/10.1098/rstb.2015.0115
26. Cerami C, Perini G, Panzavolta A, Cotta Ramusino M, Costa A. 2022. A call for drug therapies for the treatment of social behavior disorders in dementia systematic review of evidence and state of the art. Int J Mol Sci 23:11550. https://doi.org/10.3390/ijms231911550
27. Marazziti D, Diep PT, Carter S, Carbone MG. 2022. Oxytocin: an old hormone, a novel psychotropic drug and its possible use in treating psychiatric disorders. Curr Med Chem 29:5615–5687. https://doi.org/10.2174/0929867329666220727120646
28. Ignatiuk V, Izvolskaia M, Sharova V, Zakharova L. 2023. Disruptions in hypothalamic-pituitary-gonadal axis development and their IgG modulation after prenatal systemic inflammation in male rats. Int J Mol Sci 24:2726. https://doi.org/10.3390/ijms24032726
29. Barabás K, Szabó-Meleg E, Ábrahám IM. 2020. Effect of inflammation on female gonadotropin-releasing hormone (GnRH) neurons: mechanisms and consequences. Int J Mol Sci 21:529. https://doi.org/10.3390/ijms21020529
30. Mavoungou D, Poaty-Mavoungou V, Ongali B, Akoume MY, Maka G, Mavoungou E. 2005. Hypothalamic-pituitary gonadal axis and immune response imbalance during chronic filarial infections. Trop Med Int Health 10:1180–1186. https://doi.org/10.1111/j.1365-3156.2005.01499.x
31. Yoshida H, Goedert M. 2012. Phosphorylation of microtubule-associated protein tau by AMPK-related kinases. J Neurochem 120:165–176. https://doi.org/10.1111/j.1471-4159.2011.07523.x
32. Nem de Oliveira Souza I, Frost PS, França JV, Nascimento-Viana JB, Neris RLS, Freitas L, Pinheiro D, Nogueira CO, Neves G, Chimelli L, De Felice FG, Cavalheiro ÉA, Ferreira ST, Assunção-Miranda I, Figueiredo CP, Da Poian AT, Clarke JR. 2018. Acute and chronic neurological consequences of early-life Zika virus infection in mice. Sci Transl Med 10:eaar2749. https://doi.org/10.1126/scitranslmed.aar2749
33. Mavigner M, Raper J, Kovacs-Balint Z, Gumber S, O'Neal JT, Bhaumik SK, Zhang X, Habib J, Mattingly C, McDonald CE, Avanzato V, Burke MW, Magnani DM, Bailey VK, Watkins DI, Vanderford TH, Fair D, Earl E, Feczko E, Styner M, Jean SM, Cohen JK, Silvestri G, Johnson RP, O'Connor DH, Wrammert J, Suthar MS, Sanchez MM, Alvarado MC, Chahroudi A. 2018. Postnatal Zika virus infection is associated with persistent abnormalities in brain structure, function, and behavior in infant macaques. Sci Transl Med 10:eaao6975. https://doi.org/10.1126/scitranslmed.aao6975
34. Tang H, Hammack C, Ogden SC, Wen Z, Qian X, Li Y, Yao B, Shin J, Zhang F, Lee EM, Christian KM, Didier RA, Jin P, Song H, Ming GL. 2016. Zika virus infects human cortical neural progenitors and attenuates their growth. Cell Stem Cell 18:587–590. https://doi.org/10.1016/j.stem.2016.02.016
35. Christian KM, Song H, Ming GL. 2019. Pathophysiology and mechanisms of Zika virus infection in the nervous system. Annu Rev Neurosci 42:249–269. https://doi.org/10.1146/annurev-neuro-080317-062231
36. Cumberworth SL, Barrie JA, Cunningham ME, de Figueiredo DPG, Schultz V, Wilder-Smith AJ, Brennan B, Pena LJ, Freitas de Oliveira França R, Linington C, Barnett SC, Willison HJ, Kohl A, Edgar JM. 2017. Zika virus tropism and interactions in myelinating neural cell cultures: CNS cells and myelin are preferentially affected. Acta Neuropathol Commun 5:50. https://doi.org/10.1186/s40478-017-0450-8
37. Zhen ZD, Wu N, Fan DY, Ai JH, Song ZR, Chang JT, Wang PG, Wu YH, An J. 2022. Growth hormone attenuates the brain damage caused by ZIKV infection in mice. Virol Sin 37:601–609. https://doi.org/10.1016/j.virs.2022.06.004
38. Clarke IJ. 2015. Hypothalamus as an endocrine organ. Compr Physiol 5:217–253. https://doi.org/10.1002/cphy.c140019
39. Newton CL, Riekert C, Millar RP. 2018. Gonadotropin-releasing hormone analog therapeutics. Minerva Ginecol 70:497–515. https://doi.org/10.23736/S0026-4784.18.04316-2
40. Stojilkovic SS, Catt KJ. 1995. Expression and signal transduction pathways of gonadotropin-releasing hormone receptors. Recent Prog Horm Res 50:161–205. https://doi.org/10.1016/b978-0-12-571150-0.50012-3
41. Mruk DD, Cheng CY. 2015. The mammalian blood-testis barrier: Its biology and regulation. Endocr Rev 36:564–591. https://doi.org/10.1210/er.2014-1101
42. Abel MH, Wootton AN, Wilkins V, Huhtaniemi I, Knight PG, Charlton HM. 2000. The effect of a null mutation in the follicle-stimulating hormone receptor gene on mouse reproduction. Endocrinology 141:1795–1803. https://doi.org/10.1210/endo.141.5.7456
43. Sharpe RM. 2012. Sperm counts and fertility in men: a rocky road ahead. EMBO Rep 13:398–403. https://doi.org/10.1038/embor.2012.50
44. Lei ZM, Mishra S, Zou W, Xu B, Foltz M, Li X, Rao CV. 2001. Targeted disruption of luteinizing hormone/human chorionic gonadotropin receptor gene. Mol Endocrinol 15:184–200. https://doi.org/10.1210/mend.15.1.0586
45. Abel MH, Baker PJ, Charlton HM, Monteiro A, Verhoeven G, De Gendt K, Guillou F, O'Shaughnessy PJ. 2008. Spermatogenesis and sertoli cell activity in mice lacking sertoli cell receptors for follicle-stimulating hormone and androgen. Endocrinology 149:3279–3285. https://doi.org/10.1210/en.2008-0086
46. Zheng B, Sun J, Luo H, Yang L, Li Q, Zhang L, Si Y, Cao S, Ye J. 2022. Testosterone protects mice against Zika virus infection and suppresses

the inflammatory response in the brain. iScience 25:105300. https://doi.org/10.1016/j.isci.2022.105300
47. Ye X, Li F, Zhang J, Ma H, Ji D, Huang X, Curry TE, Liu W, Liu J. 2017. Pyrethroid insecticide cypermethrin accelerates pubertal onset in male mice via disrupting hypothalamic-pituitary-gonadal axis. Environ Sci Technol 51:10212–10221. https://doi.org/10.1021/acs.est.7b02739
48. Kim D, Paggi JM, Park C, Bennett C, Salzberg SL. 2019. Graph-based genome alignment and Genotyping with HISAT2 and HISAT-genotype. Nat Biotechnol 37:907–915. https://doi.org/10.1038/s41587-019-0201-4
49. Pertea M, Kim D, Pertea GM, Leek JT, Salzberg SL. 2016. Transcript-level expression analysis of RNA-seq experiments with HISAT, stringtie and ballgown. Nat Protoc 11:1650–1667. https://doi.org/10.1038/nprot.2016.095
50. Love MI, Huber W, Anders S. 2014. Moderated estimation of fold change and dispersion for RNA-seq data with DESeq2. Genome Biol 15:550. https://doi.org/10.1186/s13059-014-0550-8
51. Yu G, Wang LG, Han Y, He QY. 2012. Clusterprofiler: an R package for comparing biological themes among gene clusters. OMICS 16:284–287. https://doi.org/10.1089/omi.2011.0118
52. Yang M, Silverman JL, Crawley JN. 2011. Automated three-chambered social approach task for mice. Curr Protoc Neurosci Chapter 8:Unit 8 26. https://doi.org/10.1002/0471142301.ns0826s56
53. You R, Liu Y, Chang R-C. 2019. A behavioral test battery for the repeated assessment of motor skills, mood, and cognition in mice. J Vis Exp. https://doi.org/10.3791/58973